DESIGN OF A MOLD INSERT ALIGNMENT SYSTEM FOR DOUBLE-SIDED HOT EMBOSSING OF MICROFLUIDIC DEVICES USING KINEMATIC CONSTRAINTS

by

Timothy Glenn Conner, B. S. T.

A thesis submitted to the Graduate Council of
Texas State University in partial fulfillment
of the requirements for the degree of
Master of Science in Technology
with a Major in Industrial Technology
December 2013

Committee Members:

Byoung Hee You, Chair

In-Hyouk Song

Vedaraman Sriraman

FAIR USE AND AUTHOR'S PERMISSION STATEMENT

Fair Use

Duplication Permission

DEDICATION

I would like to dedicate this to all Coast Guard men and women past, present and future. Many of those who served before me and some who served with me inspired me to always strive to achieve my goals. I hope to have inspired others with whom I served and those who followed after in a like manner.

ACKNOWLEDGMENTS

I want to thank my committee chair and advisor, Dr. Byoung Hee You, for allowing me the opportunity to conduct this research at Texas State University and for his guidance and support. Although he always referred to me as his “senior student” his advice for me was always appreciated.

I want to thank my committee members: Dr. In-Hyouk Song and Dr. Vederaman Sriraman for the assistance they provided in this endeavor. I offer a sincere thanks to Dr Andy Batey, the Technology Department Chair, for all of the great advice and kind words throughout my time at this university. I also extend a word of thanks to the rest of the faculty who guided my education at this fine research institution.

I thank the friends I made at this school, both as an undergraduate and as a graduate student, for their help and assistance. Without the help of some of these people I could never have achieved this goal. I thank my friends outside of academia who supported my efforts and allowed me the necessary distractions to maintain my focus. Furthermore, I thank my family for putting up with this quest of mine and indulging me.

Finally, I thank my parents, Tommie and Grace Conner, for always believing in my abilities. When I had doubts, they gave me the praise I needed to keep me on track.

TABLE OF CONTENTS

Page

LIST OF TABLES

Table **Page**

LIST OF FIGURES

Figure **Page**

ABSTRACT

The fabrication of microfluidic devices using hot embossing has increased in complexity. Many systems are multi component systems requiring that each be aligned properly with its mating components. Double-sided hot embossing is often used to produce stackable components for these assemblies. Accurate alignment of the two mold inserts, and therefore the opposing faces of the substrate, is a critical aspect to successful assembly of multi-layered modules.

A cost effective alignment system based on kinematic constraints was designed, fabricated, and tested to determine the accuracy and precision of the system. Double-sided substrates were hot embossed and characterized to evaluate the effectiveness of the design.

CHAPTER I

Introduction

1.1 Motivation

Accurate mold alignment has a significant potential to successfully produce polymer microfluidic devices with double-sided patterns on the top and bottom surfaces. Double-sided hot embossing allows simultaneous transfer of features to both the top and bottom surfaces of a polymer substrate. The functional units on the surfaces can be interconnected by aligning the reservoirs and channels to transport samples and reagents. Misalignment of the fluidic interconnection between the units must be minimized to meet the required performance of the devices. Mold alignment can minimize the misalignment, enabling it to provide a path to integrate the units into a complete microfluidic device.

Polymer applications in Micro-Electrical-Mechanical Systems (MEMS) have been widely developed especially in the Biomedical or Biological MEMS field (Bio-MEMS). Smaller sample sizes and high replication quality are typical advantages of the use of polymers in MEMS (Kastantin, et al., 2003). Polymers have become popular due to the wide variety of fabrication techniques available, extensive range of physical and chemical properties, and the efficient cost of the substrate when compared to glass and silicon. The benefits of polymer over traditional materials make them desirable for biocompatible systems (Mathur, et al., 2009) and microfluidic devices (Tennico, Koesdjojo, Kondo, Mandrell, & Remcho, 2010).

Double-sided hot embossing has numerous applications. It is used in the fabrication of lab-on-a-chip (LOC) for medical and environmental diagnostic devices. Hot embossing is a manufacturing technology used to transfer features from a mold insert

into a polymer substrate. It has been widely used to fabricate polymer microstructures (Heckele & Schomburg, 2004). Effective mold exchange, adaptability to a variety of polymer substrates, high quality of replication, and low temperature cycles are typical advantages of hot embossing, making it the preferred manufacturing technique.

Hot embossing can be divided into three principle steps: molding, cooling, and demolding. During molding, designed features are transferred from the mold inserts into the polymer substrate by the use of embossing force. Molding temperatures above the glass transition temperature (T_g) of the polymer substrate are recommended to reduce fluidic resistance and promote the patterning. During cooling the mold inserts and the polymer substrate are cooled down to a temperature below the glass transition temperature of the polymer while maintaining the embossing force inducing thermal stress at the interfacial layers of the polymer and mold inserts. This reduces the likelihood of undesired deformation during demolding. Finally, the pressure is released and the sample is separated from the mold insert (Juang, Lee, & Koelling, 2002). In double-sided hot embossing there are two mold inserts and patterning is simultaneously transferred to both sides of the polymer substrate.

Double-sided hot embossing allows for the fabrication of substrates with connection features which allow stacking of multiple layers to create more complex structures. Studies have shown the ability to use exact constraints (You, et al., 2009) and elastic averaging to achieve quality alignments (Slocum & Weber, 2003). These studies used a series of balls and v-grooves (You, et al., 2009) and either three hemispheres with a flat, a v-groove, and a trihedral feature or three hemispheres and three v-grooves

(Slocum & Weber, 2003) to achieve the exact constraints to locate and fix two facing sets of features to one another.

When aligning multiple sets in this manner, some of the components need to be double-sided. Since the opposing faces are not independent of one another, alignment of the mold insert faces is required (Grund, Heckele, & Kohl, 2008). A double-sided component would need both of its faces to be properly aligned with each other and have the necessary alignment features to use the exact constraints and elastic averaging methods previously investigated. The alignment precision is dependent on the application of the components (Heckele M. , 2004). Two alignment methods are prevalent. The first is active alignment which involves monitoring the misalignment of the two components as they are brought together and providing feedback to reduce the misalignment during the process. Optical alignment used in wafer bonding uses alignment marks for this purpose (Jiang, Pandraud, French, Spearing, & Kraft, 2007). The second method is passive alignment; it uses mechanical features on the two components to interact with each other to provide alignment. The active alignment is more accurate however a passive system is cost effective due to the lack of software and hardware needed for the monitoring and feedback. A system using passive alignment requires re-machining the mold inserts if misalignment is determined. An adjustable system based on kinematics could be a hybrid alignment system drawing benefits from active and passive systems while reducing drawbacks. It would be used to constrain the device.

A hybrid system should incorporate the advantages and limit the disadvantages of both methods. Simplicity of design and operation would offset the high cost of software and equipment associated with active alignment. A simple design based on kinematic

constraints using a screw thread of 40 threads per inch will afford accuracy of at least 25 μm which is an improvement over some passive alignment systems. The ability to adjust on-the-fly eliminates the need for re-machining the mold inserts under the current passive systems. The optimal design would provide a reasonable degree of accuracy while simple to fabricate and operate, allow adjustments for misalignment, and be constructed from readily accessible, low-cost materials.

A rigid body can have six degrees of freedom in three-dimensional space. There are three translational and three rotational degrees of freedom. All six degrees of freedom must be controlled to exactly constrain the rigid body. With the three-dimensional object resting on a plane, it can be considered as a two-dimensional object since three degrees of freedom (translation along -Z and rotation about -X and -Y) are constrained. As a two-dimensional object, only three degrees of freedom are of concern: two translational and one rotational motion (Blanding, 1999). We refer the left-to-right degree of freedom, the "X degree of freedom" and the front-to-back degree of freedom, the "Y degree of freedom." Each is parallel to the X or Y axes respectively. The rotational degree of freedom is "θ_z" because it is rotational about the Z axis. A single constraint line along each of the X and Y axes will remove the X and Y translational degrees of freedom. An additional constraint along the Y axis will remove the θ_z. A system which is under constrained has one or more degrees of freedom that are not constrained. Over constraint has more constraints than required and causes problems such as internal stresses (Whitney, 2004). Exact design is one where neither under constraint not over constraint exists. The design constrains exactly the degrees of freedom that are desired (Downey, Parkinson, & Chase, 2003).

1.2 Objective

The primary objective is to design an alignment mechanism to properly align the upper and complimentary mold inserts using kinematic constraints. The alignment mechanism will further adjust for minor misalignment of the complimentary mold insert to achieve proper alignment with the upper mold insert. Finally, the alignment mechanism will be constructed from readily available materials, using available machine tools, provide the required accuracy, and be simple to operate.

1.3 Outline

The principles, methods and materials, results, and conclusions of this study are found in the following chapters.

Chapter 2 begins with double-sided microfluidic devices. It mentions some specific examples of its use. Next, the prevailing alignment methods, their principle uses, advantages and disadvantages of each are discussed. Finally, kinematic design is discussed to support the use of those principles in the design and fabrication of the alignment system.

Chapter 3 deals with the modifications made to the existing equipment. The materials used and design of the mold inserts and alignment tools are also covered here. The procedures used in alignment as well as the double-sided hot embossing steps are delineated in this chapter. The methods used to characterize the experiments are covered as well.

The results of the experiments are covered in Chapter 4. The resulting data is discussed here to explain the findings.

The conclusions and recommendations of the study are discussed in Chapter 5.

CHAPTER II

Background

2.1 Double-Sided Microfluidic Devices

Developing a microfluidic system generally requires multiple sections and all the sections interconnected forming the desired completed assembly. Some of these sections must be double-sided. Initial works in microfluidics made use of glass- or silicon-based microfluidic chips. Creating them was expensive and time consuming. Polymers are being considered more and more for use in microfluidics (Matteucci, et al., 2013).

Skafte-Pedersen et al. (2013) used a micro machined mold of Polymethyl methacrylate (PMMA) and silicon/SU-8. A layer of Polydimethylsiloxane (PDMS) was applied to produce a fluid control layer and a pneumatic control layer for a modular microfluidic device. The experiments were used to demonstrate how modular systems are favored due to the ability to tailor them to different applications without complete redesign of the entire system. The PDMS structures were created using double-sided molding (Skafte-Pedersen, Sip, Folch, & Dufva, 2013).

Stoyanov et al. (2006) used PDMS and double-sided hot embossing to produce a microfluidic device with four integrated valves and two fluidic chambers for a micro Total Analysis System (μTAS) for medical diagnosis. These μTAS systems are important in medical diagnosis applications which use volumes in the microliter and nanoliter range (Stoyanov, Tewes, Koch, & Lohndorf, 2006).

2.2 Passive and Active Alignment

Two generally accepted forms of alignment are used in industry, active and passive alignment. Active alignment requires the monitoring and adjustment of the misalignment of the two molds such that the misalignment is reduced as the mold inserts

are brought together. Passive alignment uses mechanical structures on the opposing components to provide constraints to locate them. There is no monitoring or feedback used in passive alignment.

Active alignment typically provides higher precision. Depending on the alignment system, it is in the range of one micrometer. One disadvantage to this type of alignment system is the cost. It is necessarily a complex system that requires costly software and hardware for the monitoring and feedback components. Active alignment is often used in nanoimprint lithography to produce micro lenses for use in CMOS image sensors (Glinsner, Kreindl, & Kast, 2010). Polymer based lab-on-chip systems and other microfluidic devices for medical or environmental diagnostics also utilize active alignment methods in fully automated hot embossing systems (Glinsner, et al., 2010).

Khan-Malek et al. (1998) described an alignment system to address limitations in Deep X-ray lithography (DXRL). The materials used are only translucent to visible light. This required placing the alignment window outside of the region to be patterned (Khan-Malek, Wood, Dudley, & Stadler, 1998). While adaptable for DXRL, this represents a limitation to the alignment process for hot embossing.

Three-dimensional PDMS-based microstructures are stacked to produce more complex systems. Another automatic alignment system for 3-D microfluidic channels made use of active alignment for assembly and showed positive results in reducing misalignment over that of manual alignment systems (Kim, Baek, Lee, & Lee, 2005). The heat involved in hot embossing would be problematic in using cameras for alignment.

Passive alignment is considerably less expensive due to the lack of software and hardware employed by active alignment systems. The assembly time can be reduced and

the process simplified. The trade-off is in accuracy. The structures used must be well defined and precise for passive alignment to be accurate. Passive alignment structures are used in the assembly of microfluidic devices as well as hybrid Microsystems and the parallel assembly of micro devices (You, et al., 2009). Passive alignment methods are also used in aligning semiconductor devices for bonding into three-dimensional integrated circuits (Jiang, Pandraud, French, Spearing, & Kraft, 2007).

Submicron alignment has become a major limitation in multi-wafer MEMS devices and 3-D interconnects. This alignment is achieved by mechanically positioning one wafer to another wafer using optical alignment measurement techniques. Slocum and Weber described a methodology used to passively align wafers using the principle of elastic averaging. When conducting their study, two primary alignment techniques that came to mind were kinematic and elastic averaging. Kinematics requires a system to be statically determinant meaning the number of contact points or independent constraints equals the number of degrees of freedom restrained. Elastic averaging differs in that it presupposes an over constrained condition exists, but each contact element is relatively flexible. This condition allows the elements to deform elastically when forces are applied to clamp the system and the subsequent errors average. Many methods were considered but Slocum and Weber eventually turned to LEGO blocks (LEGO is a registered trademark of the LEGO Group and LEGO Systems, Inc., Enfield, CT 06083 USA). In the study LEGO blocks were assembled repeatedly with the repeatability of the block's position measured and it was determined that LEGO blocks were more repeatable than the Coordinate Measurement Machine used to determine the repeatability of the LEGO blocks. Slocum and Weber made use of matching convex and concave features to create

the passive alignment system for wafer-to-wafer alignment based on the elastic averaging concept. Through testing the repeatability of the system was found to be in the order of 1 μm (Slocum & Weber, 2003).

Another study of passive alignment was conducted by B H You et al (2009). Focusing on the importance of alignment of fluidic interconnects in a microfluidic system this study used a kinematic pair consisting of a v-groove and hemisphere-tipped pin. These structures provided precise and repeatable alignment in manual assembly. Avoiding over- or under-constraint was emphasized. It was determined that a set of three v-grooves and hemisphere-tipped pin joints fully constrained all of the degrees of freedom of two microfluidic modules without over-constraint. (You, et al., 2009)

2.3 Kinematic Constraint

A rigid body has six parameters, three related to rotation and three related to linear motion in three-dimensional space. These parameters comprise the six degrees of freedom. Typically the motion is applied at three axes located at right angles to each other (Whitney, 2004). When a connection is made so that a degree of freedom is reduced, the object is constrained. All six degrees of freedom must be removed in order to exactly constrain the rigid body (Blanding, 1999). The term “3-2-1” is commonly used for performing this. It means that three sharp points can determine the location of a plane. A part resting on those three points will be resting on the imaginary plane that passes through them (Whitney, 2004). With the three-dimensional object resting on a plane, it can be considered as a two-dimensional object since three degrees of freedom (along -Z and about -X and -Y) are constrained (Blanding, 1999). Using the “3-2-1” model, applying two more sharp points where they are not on the original plane or a line normal

to it, an additional two degrees of freedom are constrained. A single sharp point, not located on the first plane nor passing through the lines of the other two, will remove the final degree of freedom. When the object is pressed against these points it will be exactly constrained (Whitney, 2004).

CHAPTER III

Design and Fabrication

3.1 Modifications of Hot Press

The thermal press (3893 4NE18, Carver Inc., Wabash, IN.) was used to fabricate prototype microfluidic devices. The press was modified to attach the mold inserts and alignment tooling as well as to allow for future expansion of various mold insert types and sizes. Aluminum was chosen as a plate material since it has a high heat conductivity and a low specific heat capacity. Figure 1 shows the press.

The two platens were removed for machining. As depicted in Figure 2, each platen was drilled to a depth of 0.500 inches and tapped to accommodate a ¼ x 20 UNC screw at four locations. The aluminum plates shown in Figures 3 and 4 were drilled to

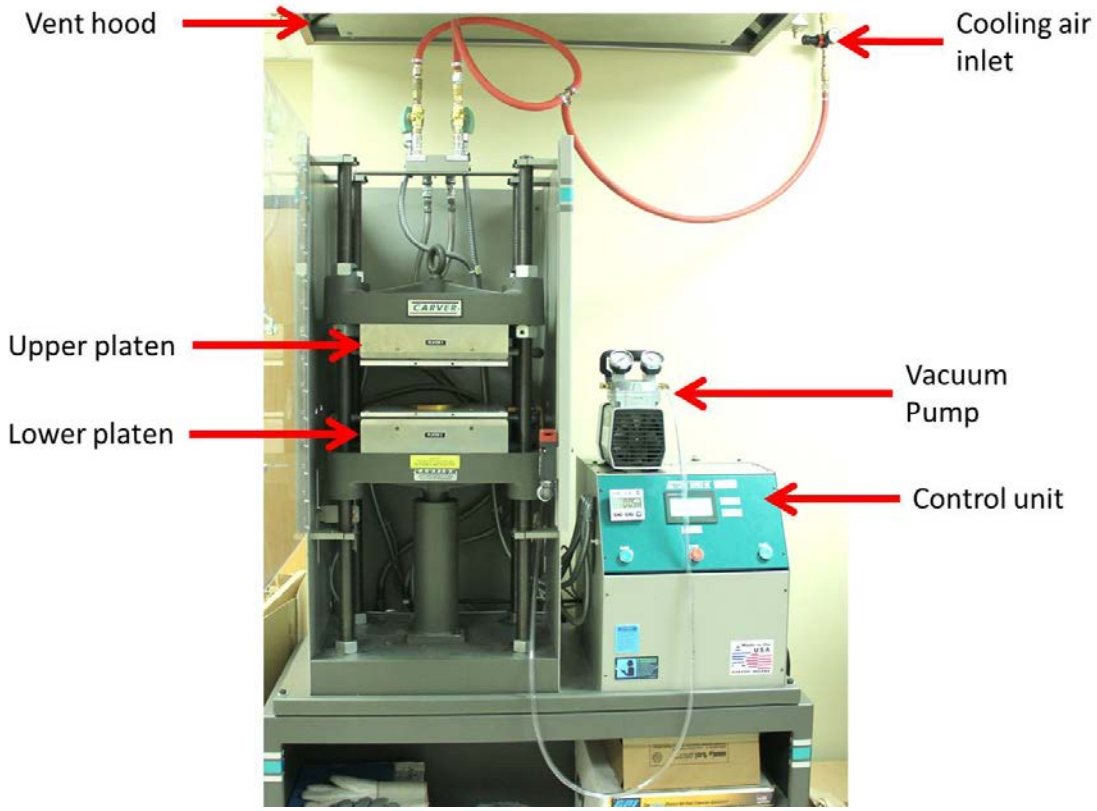

Figure 1. Carver Thermal Press 3893 4NE18 hot embossing machine.

accommodate four ¼ x 20 x ½ countersunk screws for mounting the plates to the platens. The holes were located 3 inches in from each side. Four additional holes with ¾ inch diameter were drilled at each corner to allow access to the platen mounting screws for removal of the platen with the aluminum plate attach if needed. Six holes for mounting the mold inserts were drilled into the face of each aluminum plate. These holes were drilled on a typical six bolt pattern using a 4.375 inch bolt circle and tapped for 3 mm screws. The front and left edges of the aluminum plates were drilled and tapped for 10-24 screws to mount the alignment tooling. The two holes at each location were centered and located 3 inches apart.

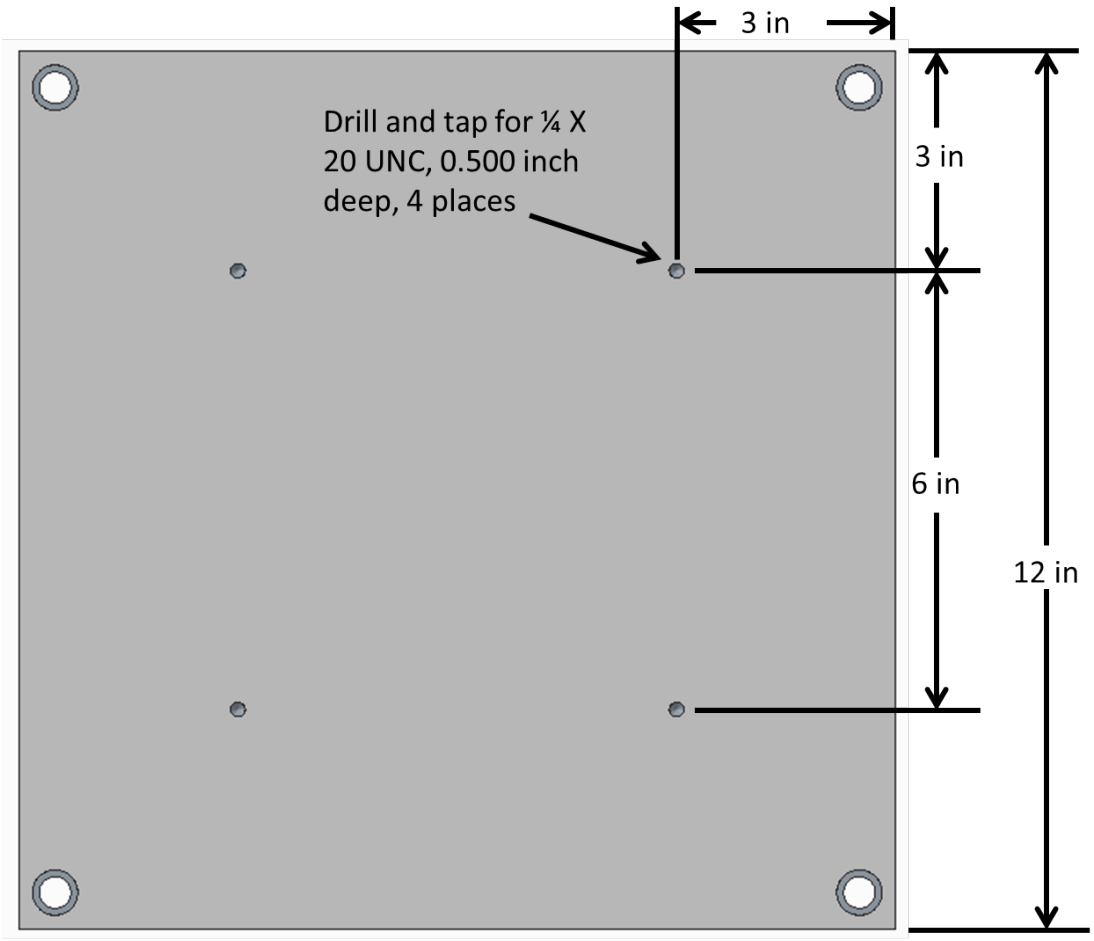

Figure 2. Modification of the heating/cooling platens.

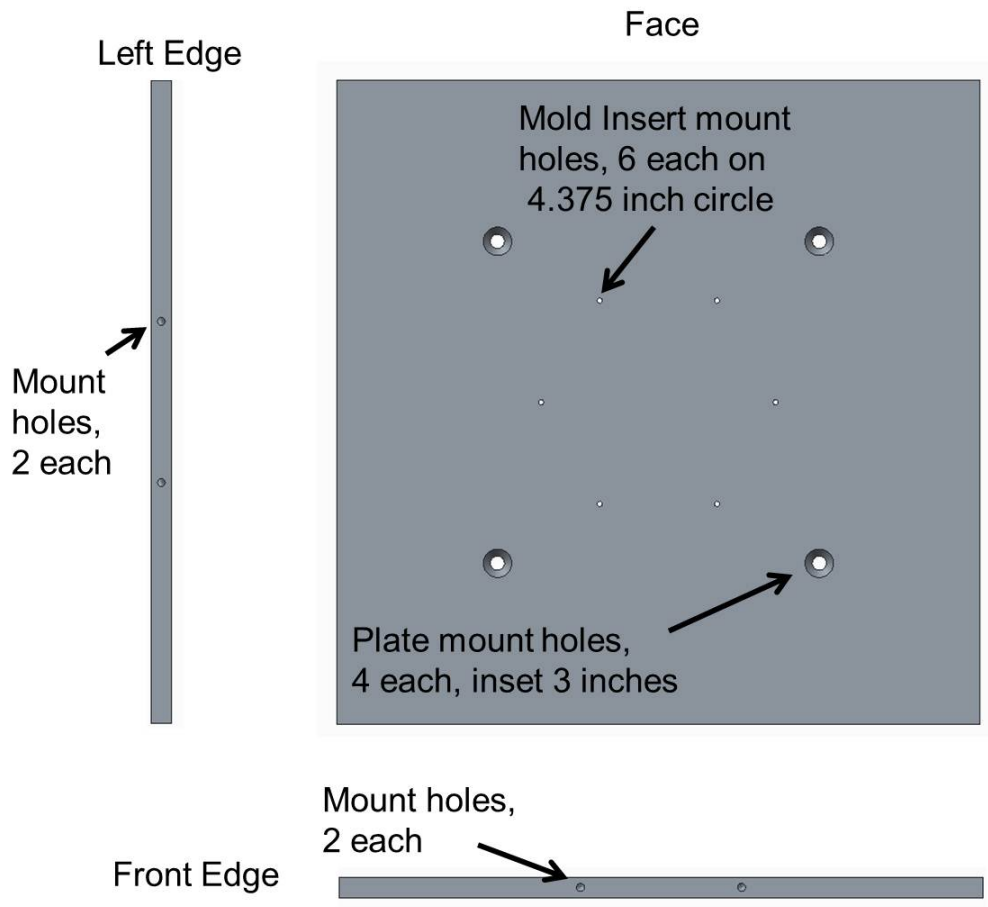

Figure 3. Top aluminum adapter plate.

The lower aluminum plate featured in Figure 4 had a feature for applying a vacuum to hold the mold insert. A hole was drilled from the center of the right edge to the center of the plate with a diameter of 0.125 inches. The end of this passage was tapped with a 1/16 National Pipe Thread (NPT) tap. Another hole was drilled in the center of the face of the plate with a diameter of 0.125 to connect with the first hole. Two concentric rings with a width and depth of 0.125 inches were machined around the face hole and joined with a groove. A vacuum pump (DOA P-704, Gast Manufacturing Inc., MI) was attached to the 1/16 NPT fitting and used to provide the vacuum to hold the complimentary mold insert in position during the embossing process.

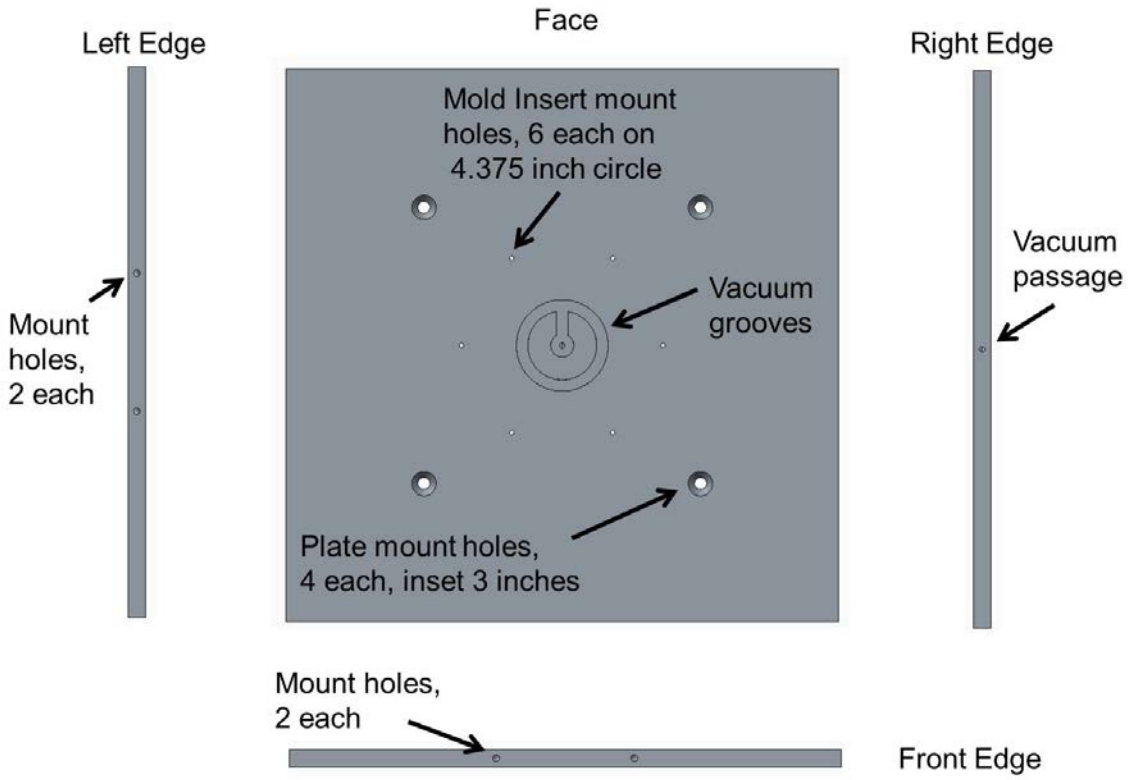

Figure 4. Bottom aluminum adapter plate.

3.2 Mold Inserts

The mold inserts were fabricated from 0.375 inch thick brass plate (P/N 8948K49, Ultra-Machinable Brass (Alloy 353), McMaster Carr, Atlanta, GA.). The patterns were generated using CAM software (Mastercam, CNC software inc., Tolland, CT.) and machined using a CNC milling machine (Minimill, Haas Automation Inc., Oxnard, CA.). The mold inserts were 4.750 inches in diameter with two short flat edges (1.0 inches long) 180° apart and one longer flat edge (1.75 inches long) 90° from the short ones as shown in Figure 5. The flat edges provided an area for the threaded rods on the alignment tools to contact. Mounting holes for 3 mm countersunk screws were drilled on a circle 4.375 inches from the center.

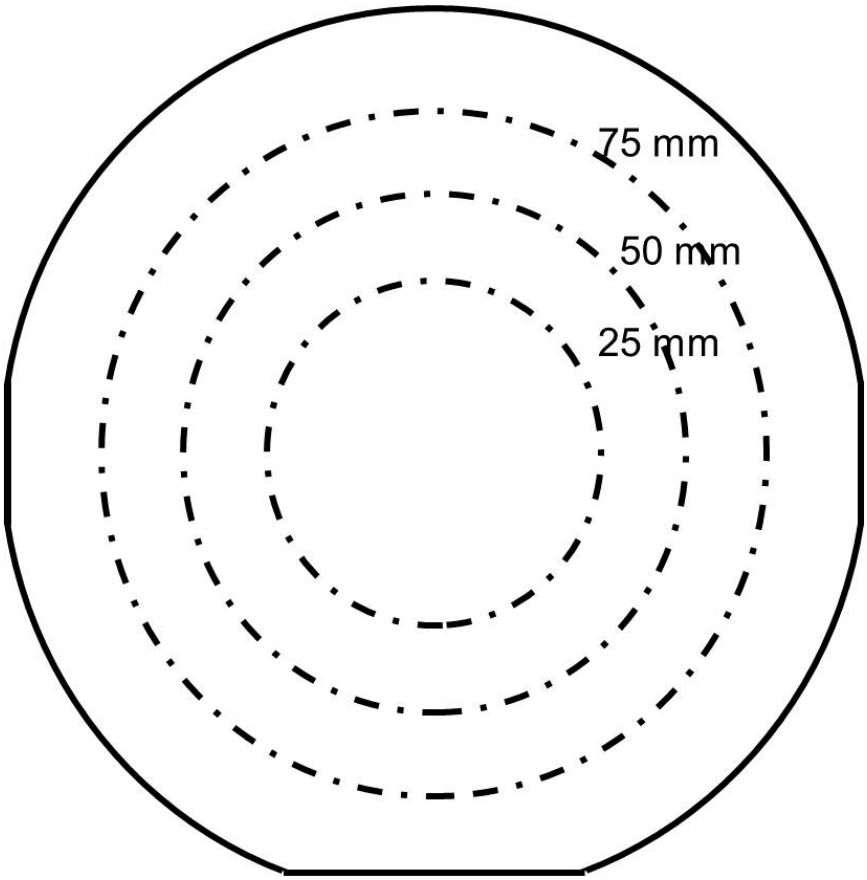

Figure 5. Outline of mold insert showing flat surfaces and 25, 50, and 75 mm circles.

Round features machined on the faces of the mold inserts depicted interconnection features of micro fluidic devices. Rectangular features were added to provide a means of rapid visible detection of misalignment. The upper mold insert depicted in Figure 6 had nine round features and eight rectangular features. The round features were 2.5 mm in diameter with a height of 0.100 mm. A single round feature was located at the center of the mold insert. Four round features were located at 90° intervals on a circle 25 mm from the center. Another four round features were located on a circle 50 mm from the center at the same 90° intervals.

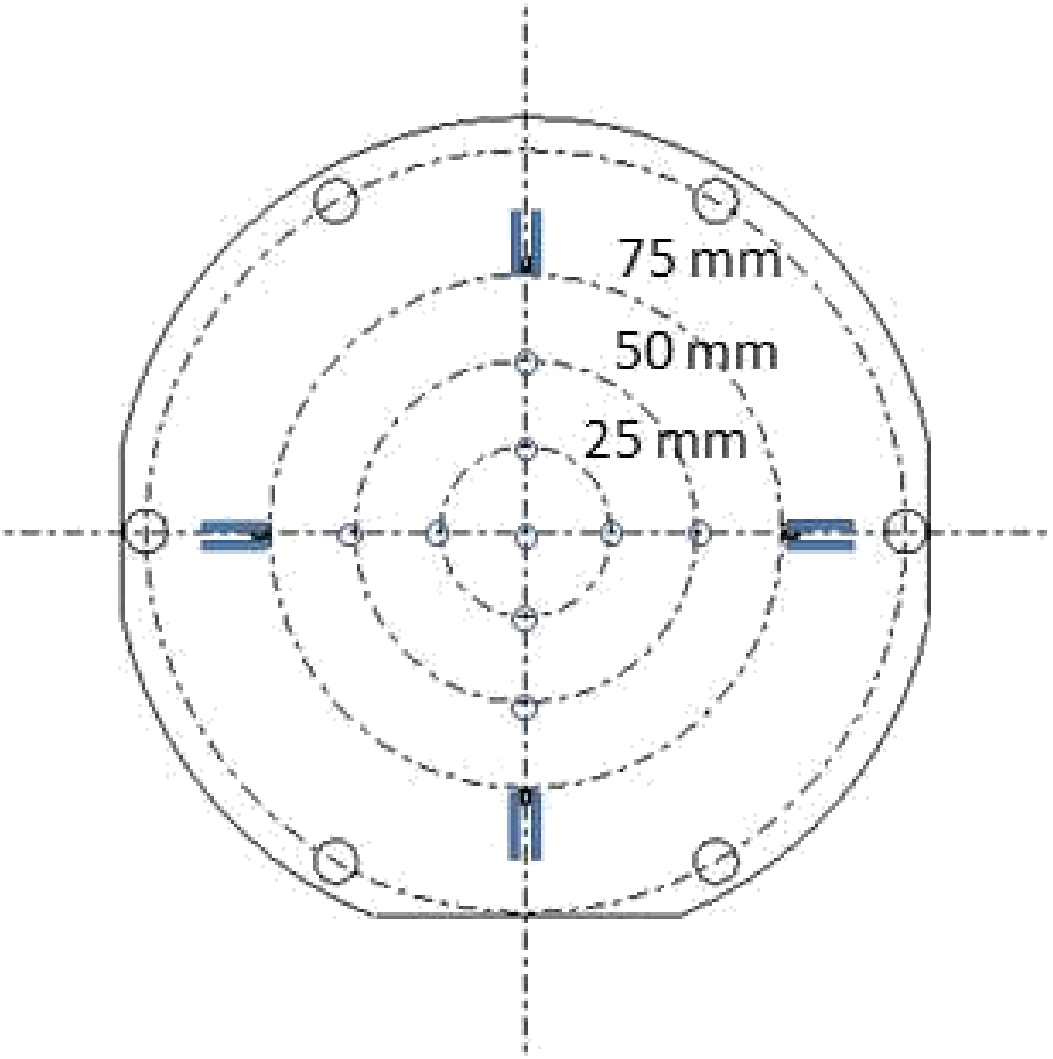

Figure 6. Depiction of the hot embossing features of the upper mold insert.

Four pairs of rectangular features were located on a circle 75 mm from the center and at the same 90° intervals. The two rectangles 0.770 mm apart were 2.50 mm long, 0.500 mm wide and 0.100 mm in height.

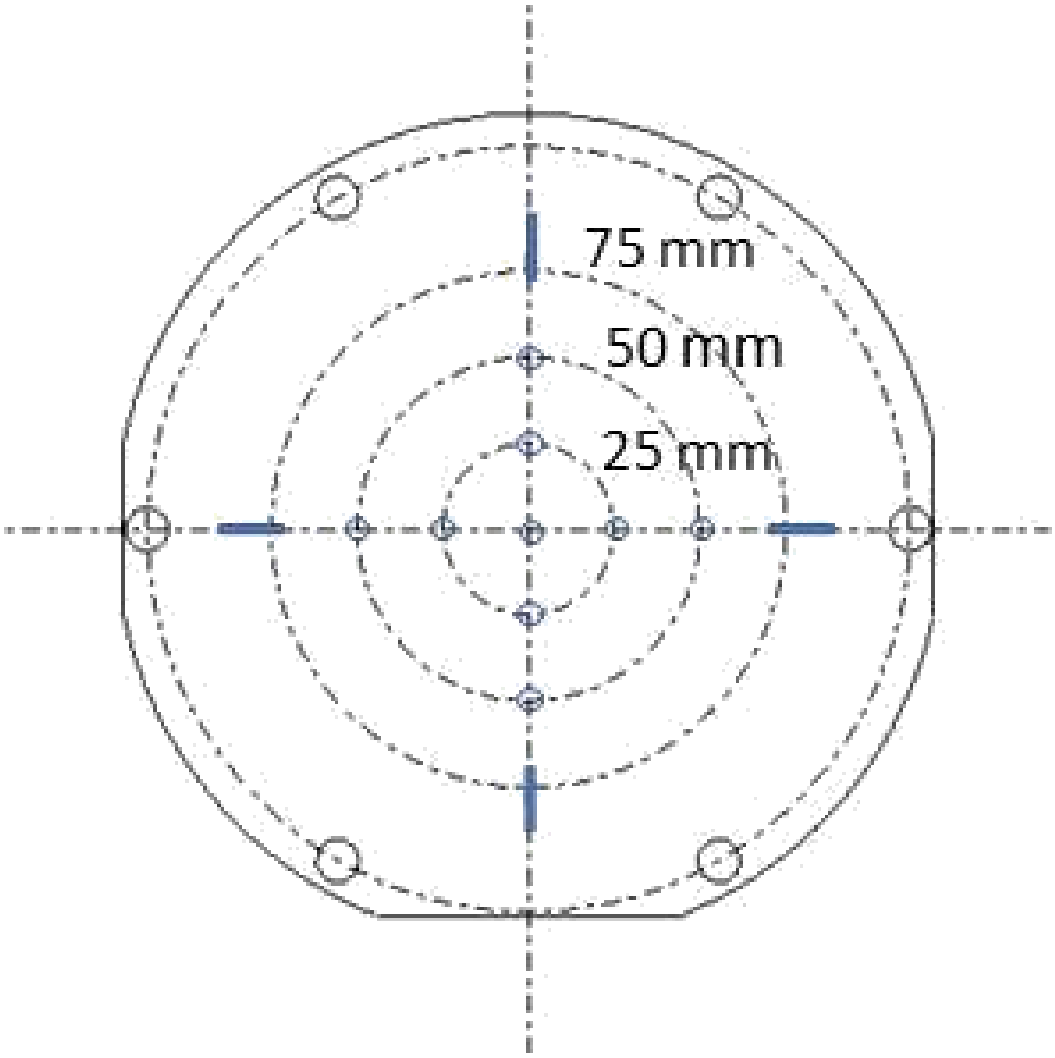

Figure 7. Depiction of the hot embossing features of the complimentary mold insert.

The complimentary mold insert in Figure 7 contained nine round and four rectangular features. The round features were 0.500 mm in diameter and 0.100 mm in height. A round feature was centered on the mold insert face with four more located on a circle 25 mm from the center and at 90° intervals. An additional four round features were located at the same 90° intervals 50 mm from the center. Four rectangular features 2.5 mm in length, 0.500 mm wide and 0.100 mm in height were located at 90 ° intervals on a circle 75 mm from the center.

The actual locations of the features from the center of the mold inserts as machined were determined to be 24.9922 ± 0.0066, 49.9947 ± .0027, and 74.9689 ± 0.0226 mm

3.3 Alignment Tools

The alignment tools shown in Figure 8, consisted of mounting plates, stiffeners, and threaded rods. The mounting plates and stiffeners were fabricated from aluminum plate. The mounting plates were 4 x 1 x 0.500 inches. Four holes were drilled using a #7 drill bit 0.500 inches from the short sides and 0.1875 inches from the long sides for mounting screws. At the center of the plate and two locations 0.500 inches to either side, holes were drilled and tapped for 5-40 threads to accommodate the threaded rods. Two additional holes were drilled along the centerline 0.750 inches to either side of center with a diameter of 0.200 inches to mount the stiffener.

The 2 x 3 inch stiffeners were “A” shaped. These were cut to shape with a water jet (Z-45 Ward Jet Inc., Tallmadge, OH.) and then milled to 0.250 inches thick. The ends of the legs were drilled and tapped for 8-32 threads for mounting to the plates. Three holes were drilled through the top of the “A” and the cross member. One was centered and the others were 0.500 inches to either side. These allowed the threaded rods to move through while providing stiffness at the extreme ends.

The threaded rods were 5-40 threads and 6 inches in length. At 40 threads per inch the rods would move in or out 0.025 inches per revolution. The threaded rods were used to determine the position the upper mold insert, relay that to position the complimentary mold insert, and adjust it if needed.

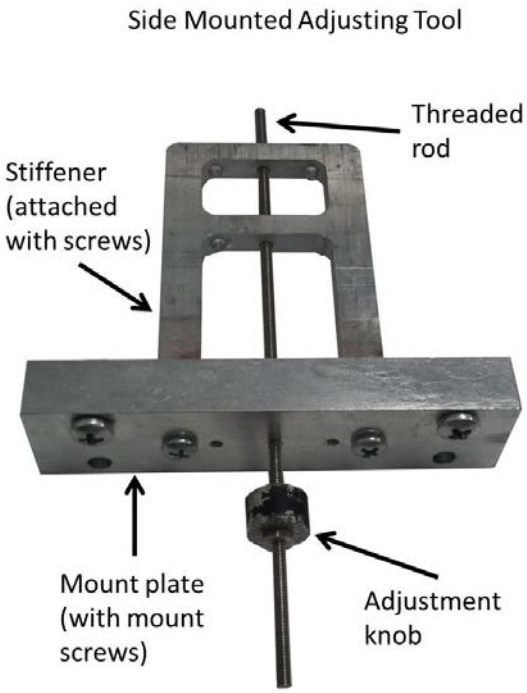

(a)

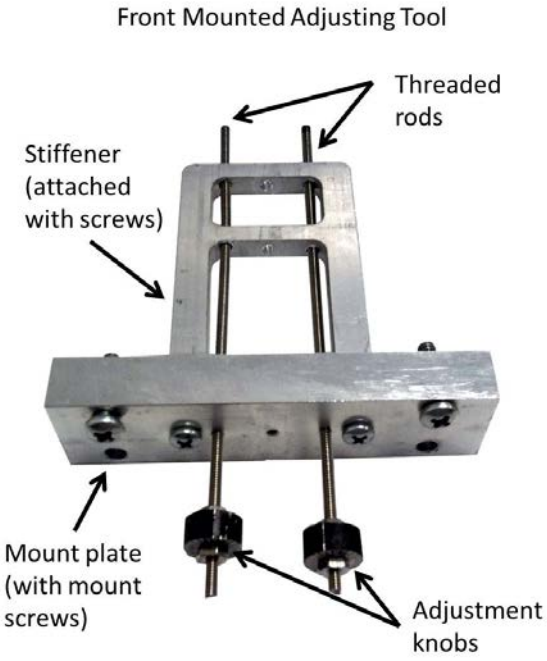

(b)

Figure 8. Alignment tools. The (a) left edge tool and (b) front edge tool.

Disks were machined 0.500 inches in diameter from 0.250 inches aluminum. These were drilled and tapped for threading into the threaded rod and acted as adjustment devices. The faces of the disks were machined with 25 equidistant marks to provide an accuracy of 0.001 inches for the tools.

The tool placed on the left edge of the press was used to position and adjust along the X axis and had one threaded rod in the center hole. The tool used on the front edge of the press determined the position along the Y axis and about the Z axis and used two threaded rods in the two outer holes.

3.4 Mold Alignment

Figure 9 a, b, c, and d depict the procedure for determining the location of the upper mold insert. The top mold insert is mounted to the upper aluminum plate with six 3 x 5 mm screws. The alignment tooling is attached to the edges of the upper plate with two 10 x 24 screws in the top mounting holes. The alignment tool on the left side has one threaded rod and the one on the front has two threaded rods. The threaded rods on the tooling are turned in until they contact the flat edges on the top mold insert. The mounting screws on the tooling are removed and the tooling moved to the lower plate where they are attached using the bottom mounting holes.

The complimentary mold insert is laid on the surface of the lower plate and brought into contact with the threaded rods on the aligning tooling. Once in place, the vacuum is applied to hold the complimentary mold insert in place. The alignment tooling is removed prior to the hot embossing (Figure 10).

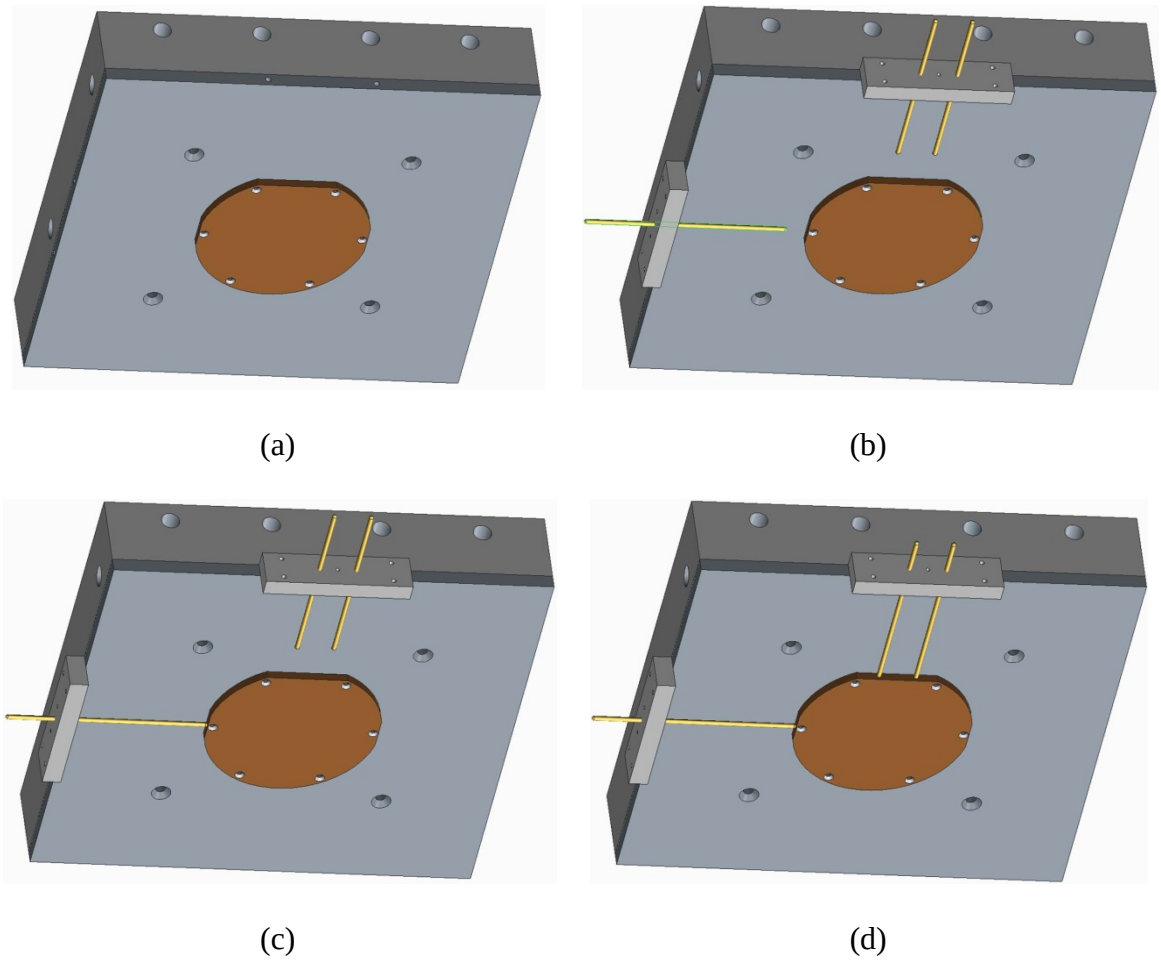

Figure 9. Depiction of the upper mold alignment procedure. To align, (a) the upper mold insert is attached by screws, (b) the alignment tools installed, (c) the left side tool brought into contact with the mold insert, and (d) the front side tool brought into contact with the mold insert.

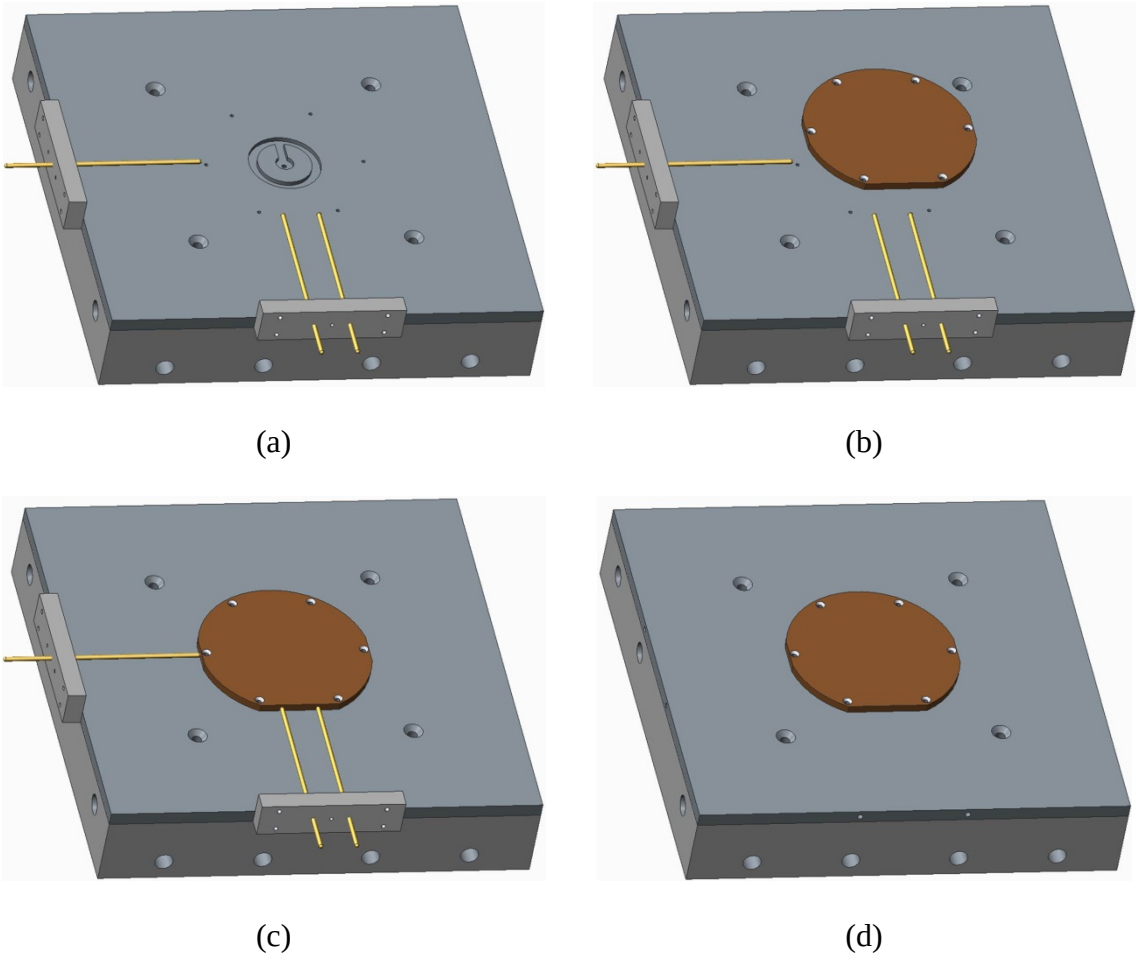

Figure 10. Depiction of the complimentary mold alignment procedure. To align, (a) the tooling is installed on the lower plate, (b) the complimentary mold insert is placed on the plate, (c) the complimentary mold insert is brought into contact with the threaded rods on the alignment tools, and (d) the alignment tools are removed prior to the hot embossing procedure.

3.5 Double-Sided Hot Embossing

Polycarbonate (Lexan®, Sabic Plastics, Shanghai, China) was the material chosen for hot embossing the experimental samples. It was preferred over PMMA because it is easier to focus through it in a microscope due to its refractive properties. PC has a T_g of 140- 150° C. The molding temperature should be above T_g in order for the polymer to flow. The embossing force is constant until de-embossing at around 15° C below T_g (Juang, Lee, & Koelling, 2002). The demolding temperature selected was 120° C. The PC

Table 1: Hot embossing parameters.

Material	PC
Molding Temperatures (°C)	170 ± 5
Embossing Forces (N)	300
Holding Times (s)	600
Demolding Temperatures (°C)	120 ± 5

was dried at 121° C for 3-24 hours in a convection oven (31-350ER-1, Quincy Lab, Chicago, IL) and sprayed with nitrogen to remove dust and particulates prior to hot embossing. The molds were sprayed with a release agent (Mold Wiz, F-57 NC, Axel Plastics Research Laboratory, Woodside, NY.) to aid in the de molding process.

Table 1 shows the process parameters used to fabricate the substrates. The platens were heated to 170° C and the substrate was positioned on the complementary mold insert. An embossing force of 300 N was applied and cooling air with an inlet pressure of 50 psi was started. Once cooled to 120° C, the press was opened and the substrate removed. The process was triplicated to determine repeatability.

3.6 Characterization

A measuring microscope (MM-800, Nikon, Japan) was used to characterize the locations of the features to determine the alignment of the molds to one another. The transparency of the PC made the top and bottom features visible without the need of turning the sample over. Due to the sizes of the features, the optimal direction of viewing was from bottom to top for proper focusing on the features. A point outside of all features was chosen to establish a consistent datum point and then three points on each circular

feature were recorded. The three points were taken at approximately 120° intervals. These positions were used to verify the center point and radius of each round feature. The calculations to determine center points and radii were performed using a Matlab formula. The differences in the locations of the center points of the top and bottom features were ascertained. The ΔX and ΔY were indicative of the amount of deviation between the mold insert positions. The local average ΔX and ΔY of each point was determined, the standard deviation was ascertained, and the 95% confidence interval was derived.

CHAPTER IV

Results and Discussion

A visual inspection of the rectangular features revealed a slight initial misalignment between the mold insert positions. The same relative misalignment was repeated in each sample. The consistency of the misalignment ruled out the possibility of unwanted movement during the hot embossing process. The data in Table 2 represents the top and bottom center points for the round features on the three samples. By subtracting the bottom reading, representing the complimentary mold insert position, from the top reading, representing the upper mold insert position, it also gives the ΔX and ΔY values for the three samples.

This data was entered into Sigma Plot and graphs of the ΔX and ΔY along the X-axis and the ΔX and ΔY along the Y-axis were generated. The initial misalignment is graphically represented in Figures 11 and 12.

Table 3 contains the data for the initial alignment of the calculated mean ΔX and ΔY values of the three samples, the standard deviation, and the 95% confidence interval. The calculated misalignment using a 95% confidence interval had a mean of 0.5976 mm ± 0.0219 mm in the positive X direction and a mean of 0.5563 mm ± 0.0791 mm in the positive Y direction.

Table 2: Derived center points for top and bottom features for the initial samples 1, 2, and 3 including calculated ΔX and ΔY values for each.

Sample #1		Quadrant 1		Quadrant 2		Quadrant 3		Quadrant 4		Center	
		X	Y	X	Y	X	Y	X	Y	X	Y
Bottom	Outer	-40.5318	17.1839	-65.9156	41.4980	-41.5908	66.8872	-16.2154	42.5876	-41.0657	42.0397
	Inner	-40.7913	29.6023	-53.4772	41.7600	-41.3319	54.4503	-28.6386	42.2987		
Top	Outer	-41.0878	16.6804	-66.4903	40.9919	-42.2176	66.3883	-16.8122	42.0655	-41.6413	41.5357
	Inner	-41.3747	29.1107	-54.0804	41.2884	-41.9348	53.9544	-29.2279	41.8128		
		DX	DY	DX	DY	DX	DY	DX	DY	DX	DY
	Outer	0.5560	0.5035	0.5747	0.5061	0.6268	0.4989	0.5968	0.5221	0.5756	0.5040
	Inner	0.5834	0.4916	0.6032	0.4716	0.6029	0.4959	0.5893	0.4859		
Sample #2		X	Y	X	Y	X	Y	X	Y	X	Y
Bottom	Outer	-43.0154	18.0540	-67.8568	42.8915	-43.0048	67.7581	-18.1570	42.9219	-43.0010	42.9125
	Inner	-43.0151	30.4762	-55.4301	42.8999	-43.0001	55.3441	-30.5841	42.8960		
Top	Outer	-43.5942	17.3975	-68.4628	42.2239	-43.6416	67.1256	-18.7477	42.3488	-43.6084	42.2637
	Inner	-43.5902	29.8441	-56.0306	42.2473	-43.6188	54.6815	-31.1685	42.3292		
		DX	DY	DX	DY	DX	DY	DX	DY	DX	DY
	Outer	0.5788	0.6565	0.6060	0.6676	0.6368	0.6325	0.5907	0.5731	0.6074	0.6488
	Inner	0.5751	0.6321	0.6005	0.6526	0.6187	0.6626	0.5844	0.5668		
Sample #3		X	Y	X	Y	X	Y	X	Y	X	Y
Bottom	Outer	-40.8882	17.4107	-65.8589	42.1434	-41.1217	67.1261	-16.1561	42.4003	-41.0030	42.1760
	Inner	-40.9536	29.8485	-53.4472	42.1942	-41.0539	54.7078	-28.5899	42.3310		
Top	Outer	-41.4881	16.8670	-66.4563	41.6126	-41.7387	66.5987	-16.7436	41.8778	-41.7081	41.6174
	Inner	-41.5199	29.2793	-53.9960	41.6698	-41.6630	54.1638	-29.1882	41.8026		
		DX	DY	DX	DY	DX	DY	DX	DY	DX	DY
	Outer	0.5999	0.5437	0.5974	0.5308	0.6170	0.5274	0.5875	0.5225	0.7051	0.5586
	Inner	0.5663	0.5692	0.5488	0.5244	0.6091	0.5440	0.5983	0.5284		

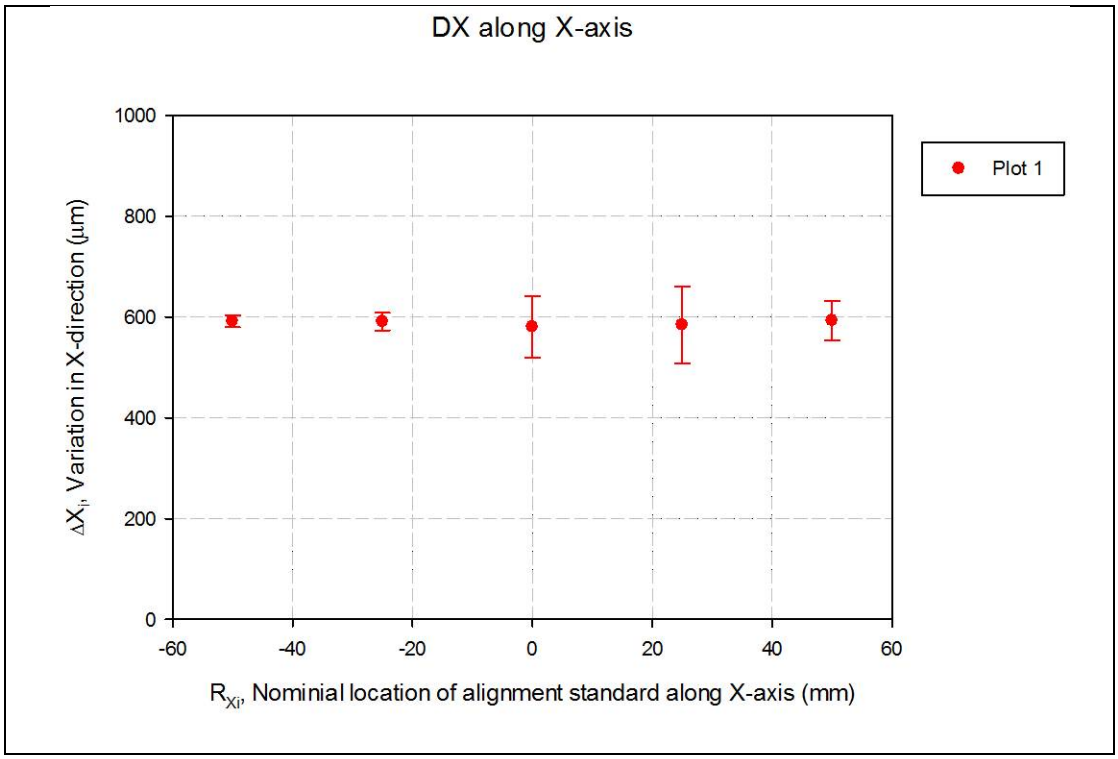

(a)

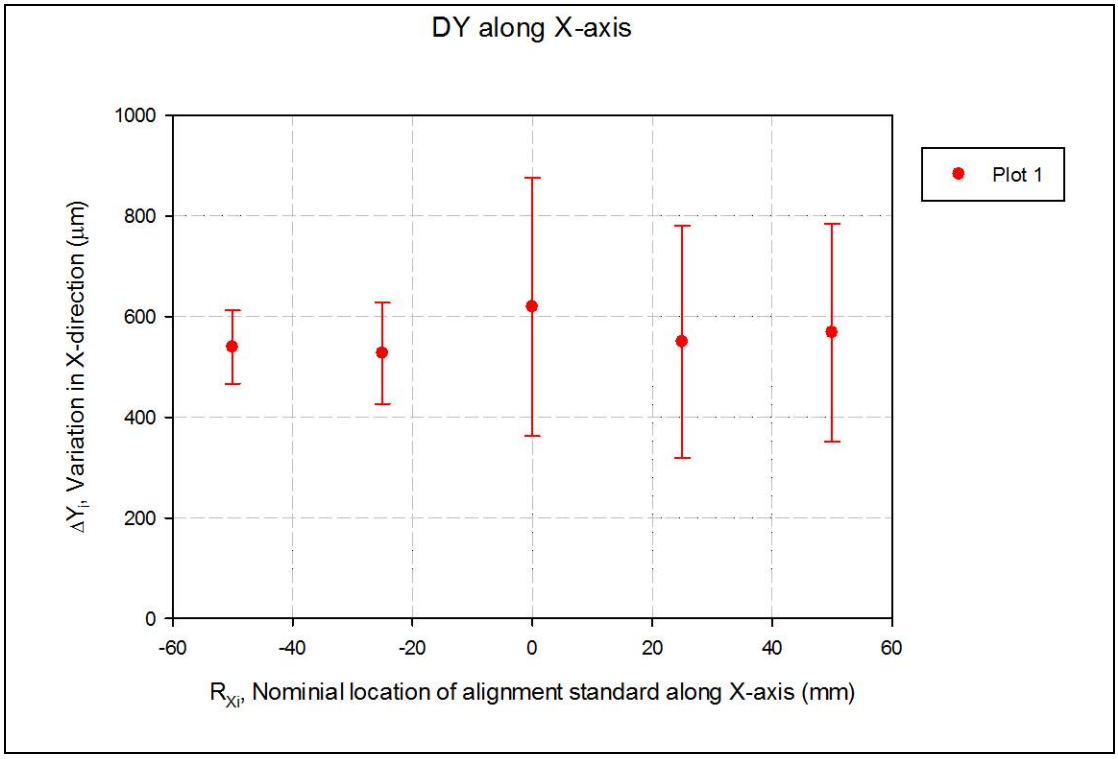

(b)

Figure 11. Graphs of deltas along X-axis of initial samples.

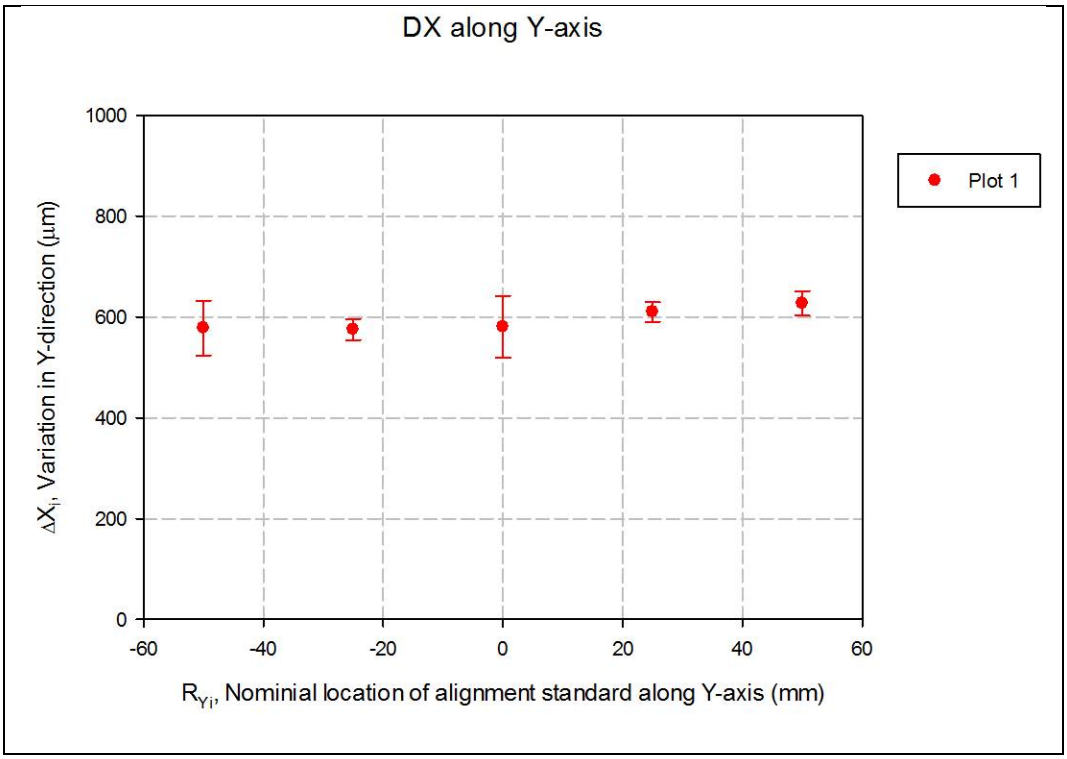

(a)

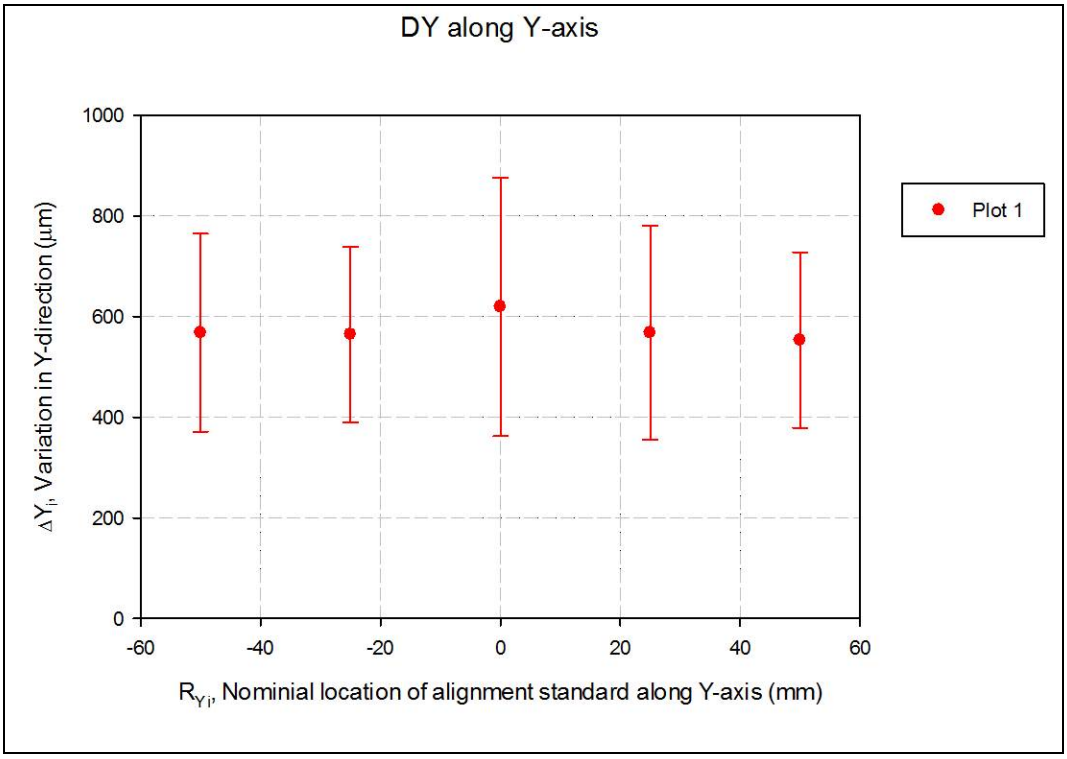

(b)

Figure 12. Graphs of deltas along Y-axis of initial samples.

Table 3: Initial alignment data. The Calculated Mean, Standard Deviation, and 95% Confidence Intervals for (a) ΔX and (b) ΔY.

		ΔX					
		Sample 1	Sample 2	Sample 3	Average	Std Dev	95% CI
Quadrant 1	Outer	0.5560	0.5788	0.5999	0.5782	0.0220	0.0248
	Inner	0.5834	0.5751	0.5663	0.5749	0.0086	0.0097
Quadrant 2	Outer	0.5747	0.6060	0.5974	0.5927	0.0162	0.0183
	Inner	0.6032	0.6005	0.5488	0.5842	0.0307	0.0347
Quadrant 3	Outer	0.6268	0.6368	0.6170	0.6269	0.0099	0.0112
	Inner	0.6029	0.6187	0.6091	0.6102	0.0080	0.0090
Quadrant 4	Outer	0.5968	0.5907	0.5875	0.5917	0.0047	0.0053
	Inner	0.5893	0.5844	0.5983	0.5907	0.0071	0.0080
	Center	0.5756	0.6074	0.7051	0.5805	0.0248	0.0280
					0.5976		0.0219

(a)

		ΔY					
		Sample 1	Sample 2	Sample 3	Average	Std Dev	95% CI
Quadrant 1	Outer	0.5035	0.6565	0.5437	0.5679	0.0793	0.0898
	Inner	0.4916	0.6321	0.5692	0.5643	0.0704	0.0796
Quadrant 2	Outer	0.5061	0.6676	0.5308	0.5682	0.0870	0.0984
	Inner	0.4716	0.6526	0.5244	0.5495	0.0931	0.1053
Quadrant 3	Outer	0.4989	0.6325	0.5274	0.5529	0.0704	0.0796
	Inner	0.4959	0.6626	0.5440	0.5675	0.0858	0.0971
Quadrant 4	Outer	0.5221	0.5731	0.5225	0.5392	0.0293	0.0332
	Inner	0.4859	0.5668	0.5284	0.5270	0.0405	0.0458
	Center	0.5040	0.6488	0.5586	0.6193	0.1037	0.1174
					0.5563		0.0791

(b)

Photos were taken of the three substrates showing the original misalignment of specific features under a microscope. These photos were overlapped show an enlarged view of the misalignment. Figure 13 shows overlapped photos of the center location on the sample 1.

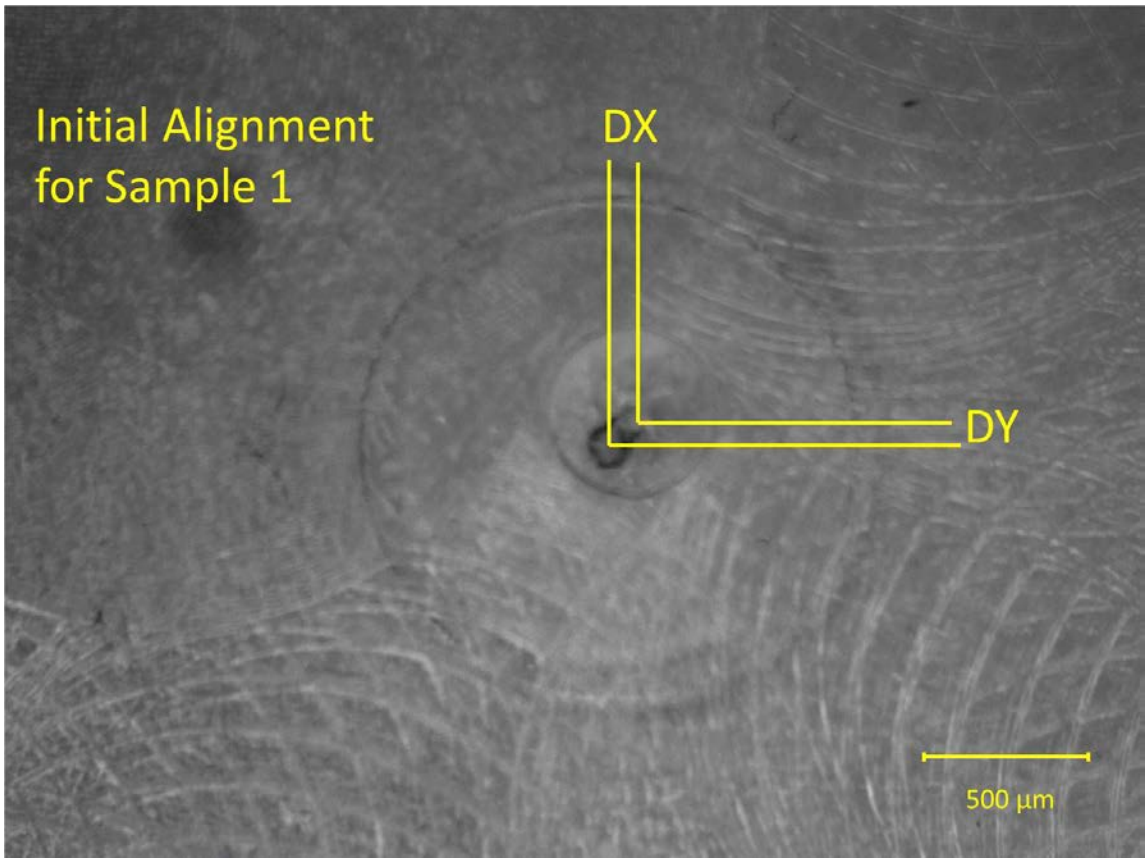

Figure 13. Microscope photos of center features (top and bottom) of sample 1 depicting the initial alignment.

With the threaded rod capable of 0.025 inches per revolution, the threaded rods were adjusted to compensate for the misalignment. Table 4 shows the calculations used to determine the adjustments to the alignment tools. The pin for the X direction was turned 23 marks in the negative X direction. The two pins for the Y direction were each turned 22 marks in the negative Y direction.

The pins on the aligning tool were adjusted according to the calculated ΔX and ΔY. The aligning tools were mounted to the lower plate. The lower mold was brought into contact with the pins and held in place with the vacuum system. Three additional substrates were hot embossed using the same process parameters as before.

Table 4: Calculations used to determine number of marks to adjust dial on alignment tools.

	mm	inches	Marks on dial
∆X	0.5976	0.0235	23
∆Y	0.5563	0.0219	22

Characterization of the samples performed using the same methods as before produced the results shown in Table 5. The table represents the top and bottom center points for the round features on the three samples. By subtracting the bottom reading, representing the complimentary mold insert position, from the top reading, representing the upper mold insert position, it also gives the ∆X and ∆Y values for the three samples.

This data was entered into Sigma Plot and graphs of the ∆X and ∆Y along the X-axis and the ∆X and ∆Y along the Y-axis were generated. The initial misalignment compared with the corrected alignment is graphically represented in Figures 14 and 15.

Table 6 contains the data for the corrected alignment for the calculated mean ∆X and ∆Y values of the three corrected samples, the standard deviation, and the 95% confidence interval. The calculated misalignment using a 95% confidence interval had a mean of 0.0540 mm ± 0.0439 mm in the positive X direction and a mean of 0.0441 mm ± 0.0685 mm in the negative Y.

Table 5: Derived center points for top and bottom features for the corrected samples 4, 5, and 6 including calculated ΔX and ΔY values for each.

Sample #4		Quadrant 1		Quadrant 2		Quadrant 3		Quadrant 4		Center	
		X	Y	X	Y	X	Y	X	Y	X	Y
Bottom	Outer	-42.6794	16.9429	-66.5437	42.7391	-40.7322	66.6020	-16.8866	40.8346	-41.7101	41.7916
	Inner	-42.1936	29.3560	-54.1286	42.2604	-41.2265	54.1820	-29.2995	41.3048		
Top	Outer	-42.5902	16.9554	-66.6187	42.5987	-40.9990	66.6467	-16.9474	41.0200	-41.7848	41.8031
	Inner	-42.1926	29.3808	-54.1954	42.1931	-41.4026	54.2196	-29.3635	41.4004		
		DX	DY	DX	DY	DX	DY	DX	DY	DX	DY
	Outer	0.0892	0.0125	-0.0750	-0.1404	-0.2668	0.0447	-0.0608	0.1854	-0.0747	0.0115
	Inner	0.0010	0.0248	-0.0668	-0.0673	-0.1761	0.0376	-0.0640	0.0956		

Sample #5		Quadrant 1		Quadrant 2		Quadrant 3		Quadrant 4		Center	
		X	Y	X	Y	X	Y	X	Y	X	Y
Bottom	Outer	-41.7171	16.9220	-66.4971	41.8589	-41.5273	66.6348	-16.7627	41.6720	-41.6195	41.7663
	Inner	-41.6789	29.3448	-54.0590	41.8049	-41.5727	54.2127	-29.1972	41.7204		
Top	Outer	-41.6870	16.8736	-66.5181	41.8717	-41.6021	66.6442	-16.8438	41.7076	-41.6507	41.7779
	Inner	-41.7216	29.3731	-54.0995	41.8468	-41.6424	54.2061	-29.2663	41.7660		
		DX	DY	DX	DY	DX	DY	DX	DY	DX	DY
	Outer	0.0301	-0.0484	-0.0210	0.0128	-0.0748	0.0094	-0.0811	0.0356	-0.0312	0.0116
	Inner	-0.0427	0.0283	-0.0405	0.0419	-0.0697	-0.0066	-0.0691	0.0456		

Sample #6		Quadrant 1		Quadrant 2		Quadrant 3		Quadrant 4		Center	
		X	Y	X	Y	X	Y	X	Y	X	Y
Bottom	Outer	-41.9398	16.8320	-66.9236	41.5453	-42.2025	66.5747	-17.2217	41.8137	-42.0713	41.6858
	Inner	-41.9944	29.2479	-54.4945	41.6115	-42.1418	54.1273	-29.6442	41.7510		
Top	Outer	-41.9462	16.9495	-66.9395	41.5896	-42.2841	66.6419	-17.2633	41.9471	-42.1134	41.7861
	Inner	-42.0204	29.3472	-54.5510	41.7035	-42.1789	54.1954	-29.6982	41.8853		
		DX	DY	DX	DY	DX	DY	DX	DY	DX	DY
	Outer	-0.0064	0.1175	-0.0159	0.0443	-0.0816	0.0672	-0.0416	0.1334	-0.0421	0.1003
	Inner	-0.0260	0.0993	-0.0565	0.0920	-0.0371	0.0681	-0.0540	0.1343		

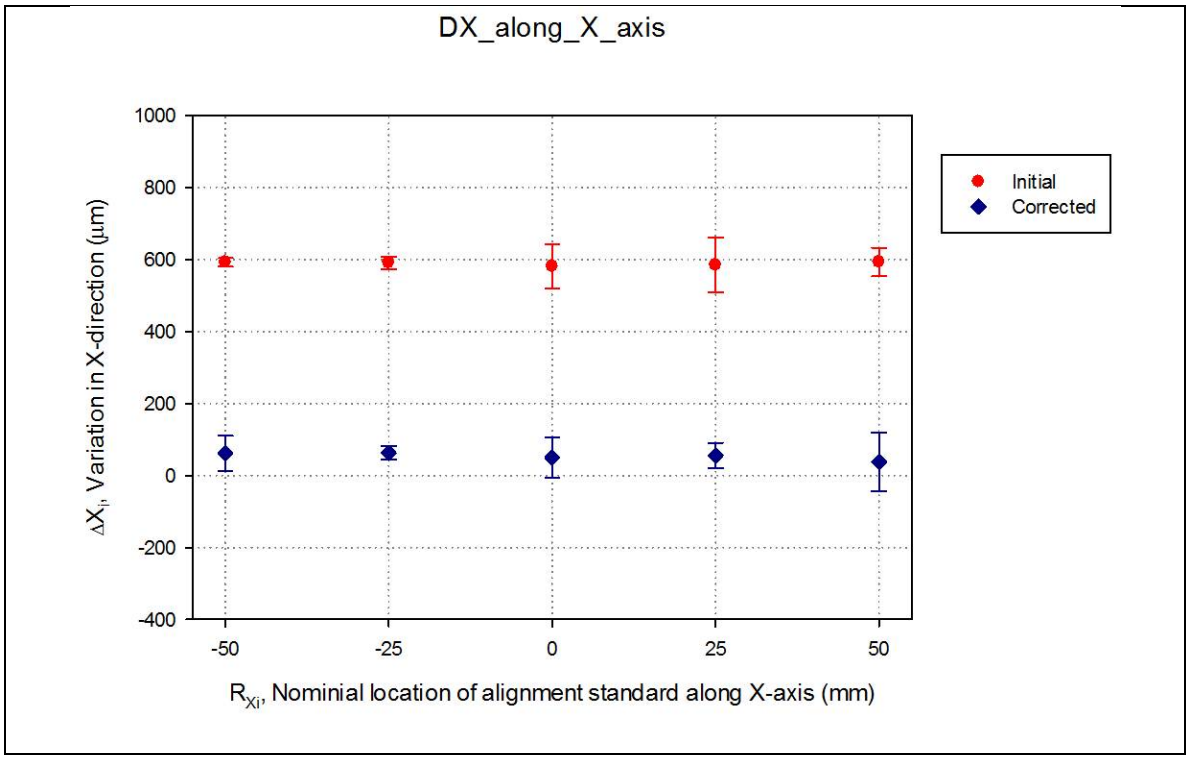

(a)

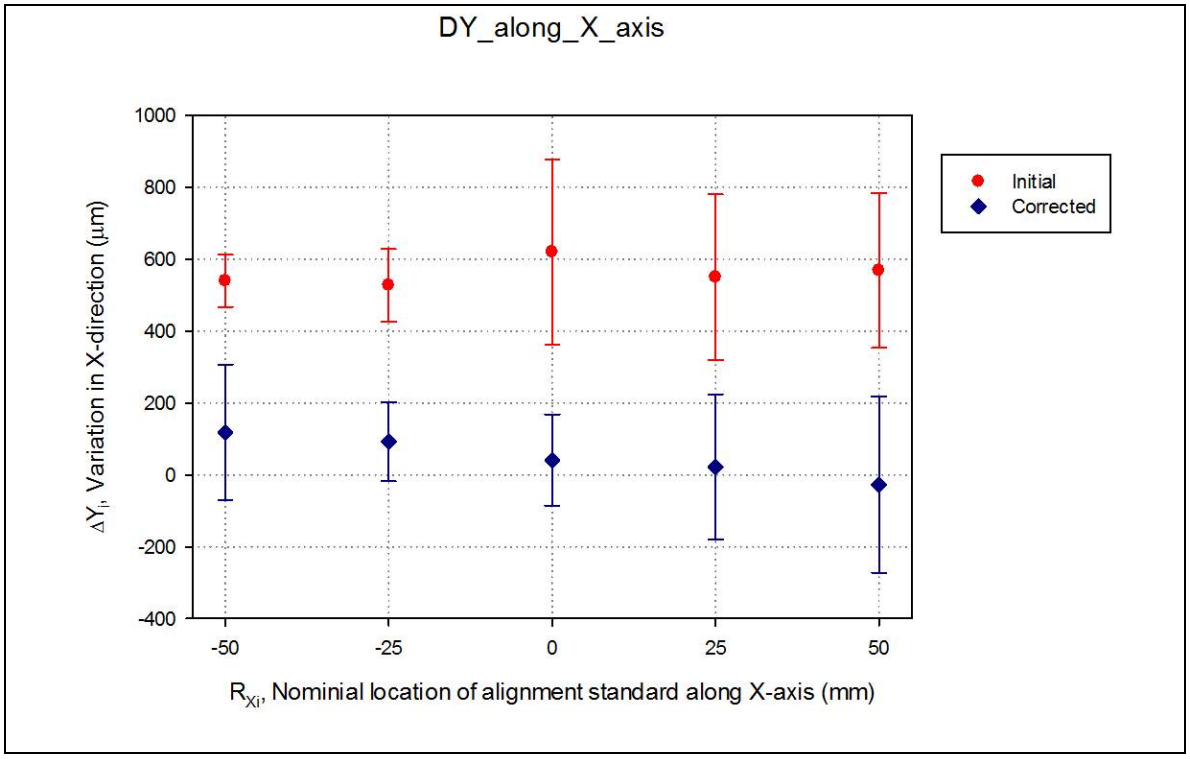

(b)

Figure 14. Comparative graphs of deltas along X-axis of both sets of samples.

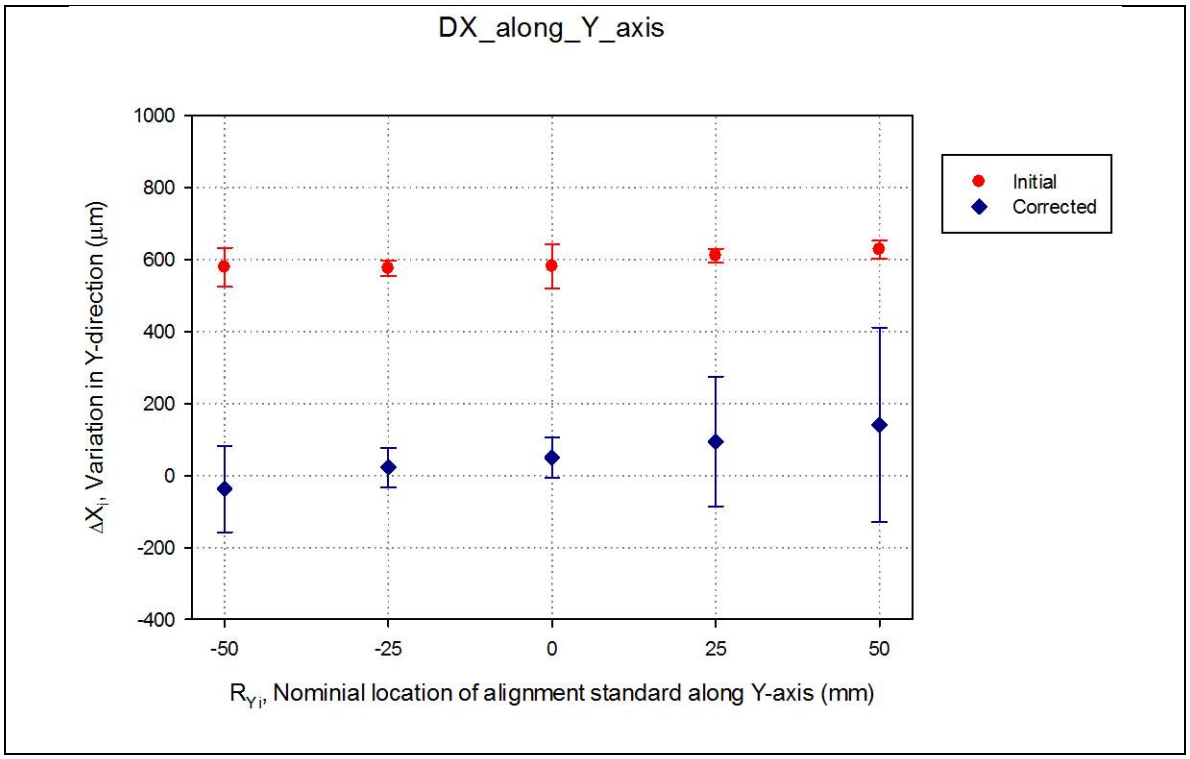

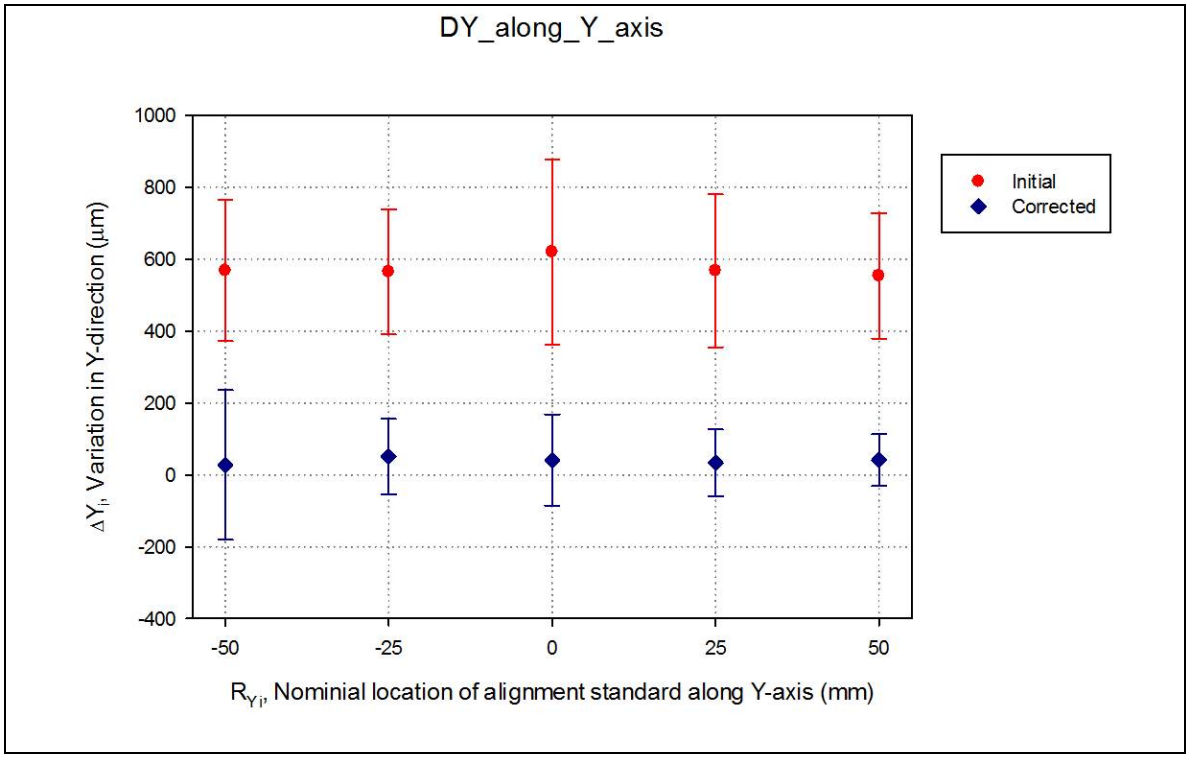

Figure 15. Comparative graphs of deltas along Y-axis of both sets of samples.

Table 6: Corrected alignment data. The Calculated Mean, Standard Deviation, and 95% Confidence Intervals for (a) ΔX and (b) ΔY.

		ΔX					
		Sample 4	Sample 5	Sample 6	Average	Std Dev	95% CI
Quadrant 1	Outer	-0.0892	-0.0301	0.0064	-0.0376	0.0482	0.0546
	Inner	-0.0010	0.0427	0.0260	0.0226	0.0221	0.0250
Quadrant 2	Outer	0.0750	0.0210	0.0159	0.0373	0.0327	0.0371
	Inner	0.0688	0.0405	0.0565	0.0553	0.0142	0.0161
Quadrant 3	Outer	0.2668	0.0748	0.0816	0.1411	0.1089	0.1233
	Inner	0.1761	0.0697	0.0371	0.0943	0.0727	0.0823
Quadrant 4	Outer	0.0608	0.0811	0.0416	0.0612	0.0198	0.0224
	Inner	0.0640	0.0691	0.0540	0.0624	0.0077	0.0087
	Center	0.0747	0.0312	0.0421	0.0493	0.0226	0.0256
					0.0540		0.0439

(a)

		ΔY					
		Sample 4	Sample 5	Sample 6	Average	Std Dev	95% CI
Quadrant 1	Outer	-0.0125	0.0484	-0.1175	-0.0272	0.0839	0.0950
	Inner	-0.0248	-0.0283	-0.0993	-0.0508	0.0420	0.0476
Quadrant 2	Outer	0.1404	-0.0128	-0.0443	0.0278	0.0988	0.1118
	Inner	0.0673	-0.0419	-0.0920	-0.0222	0.0815	0.0922
Quadrant 3	Outer	-0.0447	-0.0094	-0.0672	-0.0404	0.0291	0.0330
	Inner	-0.0376	0.0066	-0.0681	-0.0330	0.0376	0.0425
Quadrant 4	Outer	-0.1854	-0.0356	-0.1334	-0.1181	0.0761	0.0861
	Inner	-0.0956	-0.0456	-0.1343	-0.0918	0.0445	0.0503
	Center	-0.0115	-0.0116	-0.1003	-0.0411	0.0512	0.0580
					-0.0441		0.0685

(b)

Photos were taken of some of the features under a microscope. These were overlapped to show an enlarged view of the corrected alignment. Figure 16 shows overlapped photos of the center location on a representative sample.

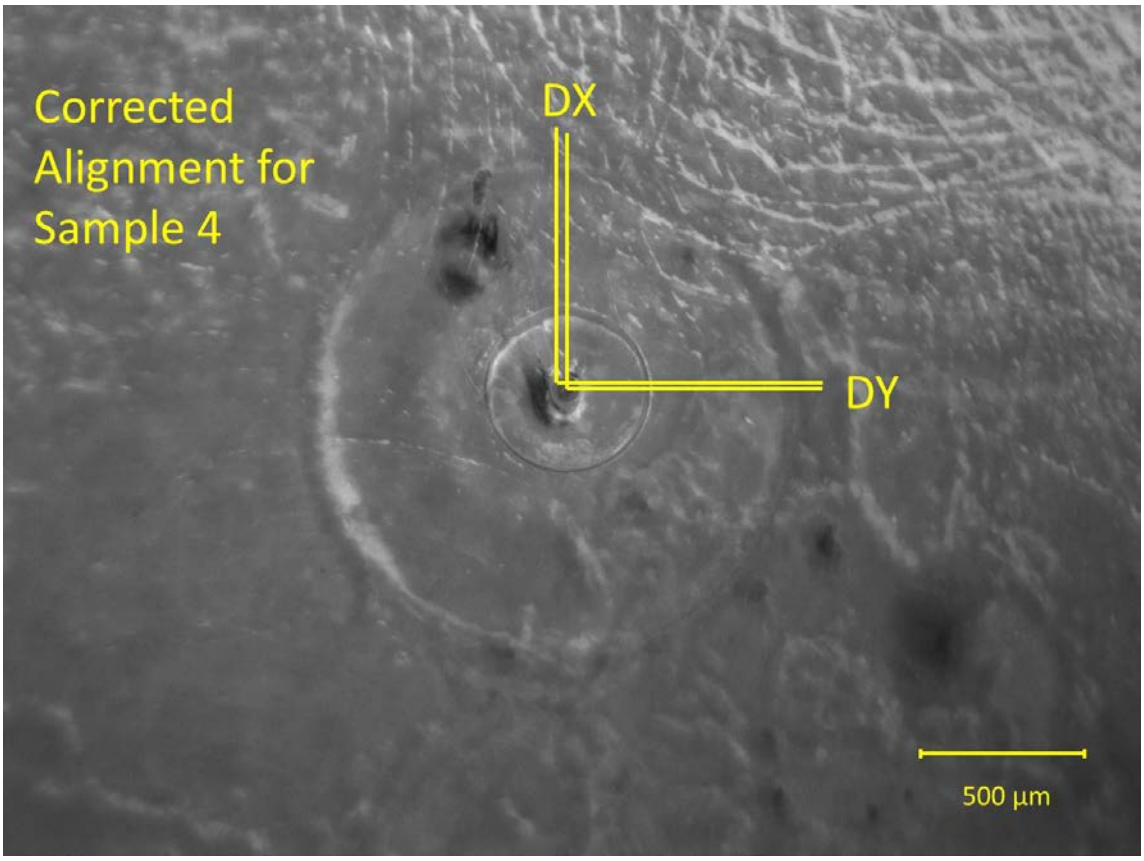

Figure 16. Microscope photos of center features (top and bottom) of sample 4 after corrective adjustments were made.

CHAPTER V

Conclusions and Recommendations

The alignment mechanism of the mold insert was demonstrated for double-sided hot embossing for microfluidic device applications. The complimentary mold insert on the lower platen was aligned with respect to the mold insert on the upper platen. The repeatability of the positioning showed that the kinematic design was effective in positioning the complimentary mold insert. The alignment tooling corrected for the initial misalignment and made an improvement to the initial positioning. Based on a 95% confidence interval the corrected alignment improved approximately 92% over the initial placement of the mold insert. The alignment mechanism was fabricated using simple machine tools in a cost effective manner from readily obtainable materials. It proved easy to use and simple to operate.

The alignment tooling showed effective precision but the accuracy could be improved. As a function of the 40 threads per inch on the threaded rod and the 25 equidistant marks on the adjustment knob, the accuracy was approximately 25.4 μm. By increasing the number of marks on the adjusting knobs or increasing the number of threads per inch on the threaded rods the accuracy of the tooling could be enhanced. Another recommendation is to develop an improved platen cooling system to reduce the cooling time of the press in order to improve the overall cycle time.

APPENDIX SECTION

APPENDIX A

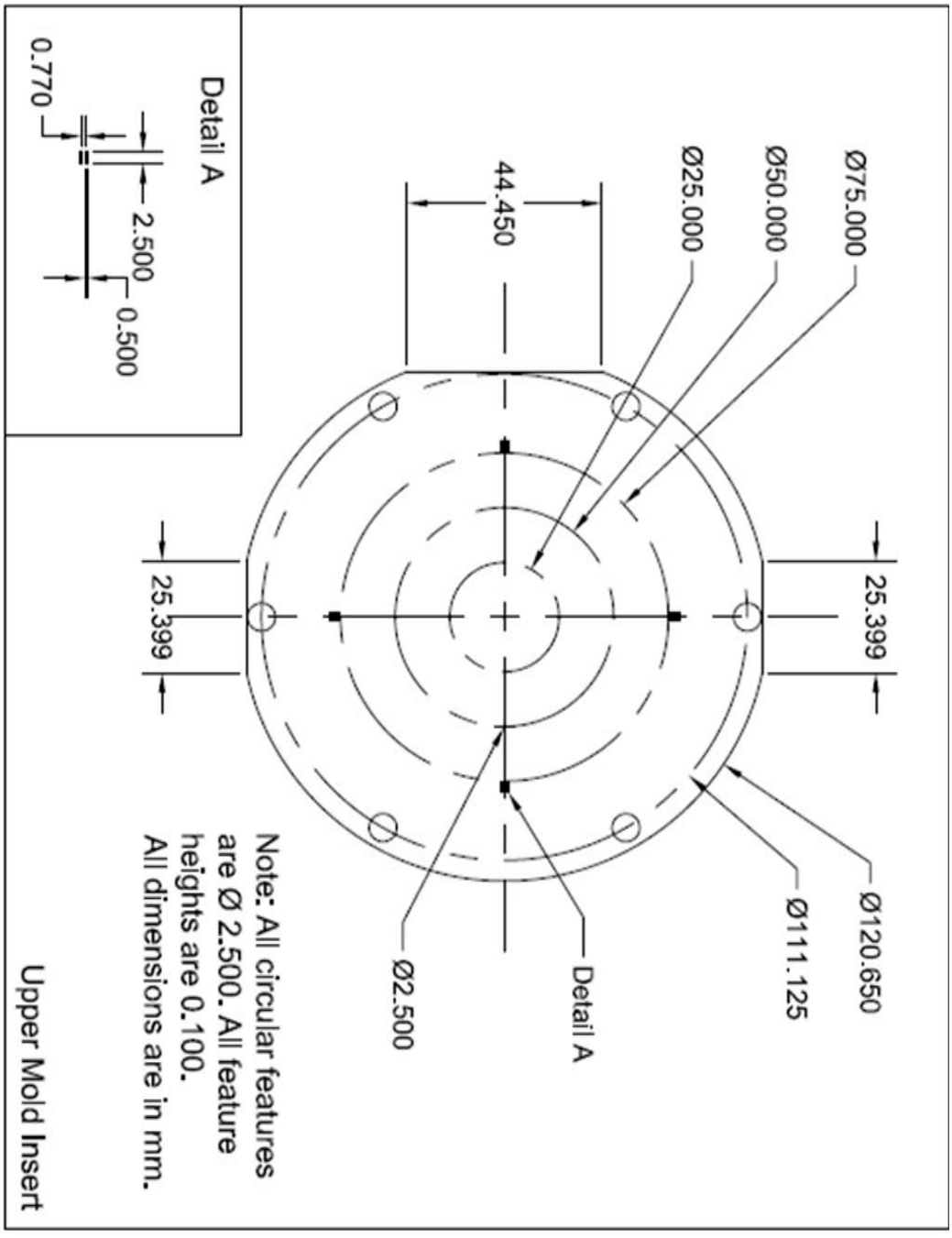

Drawing of Upper Mold Insert showing all critical dimensions of features.

APPENDIX B

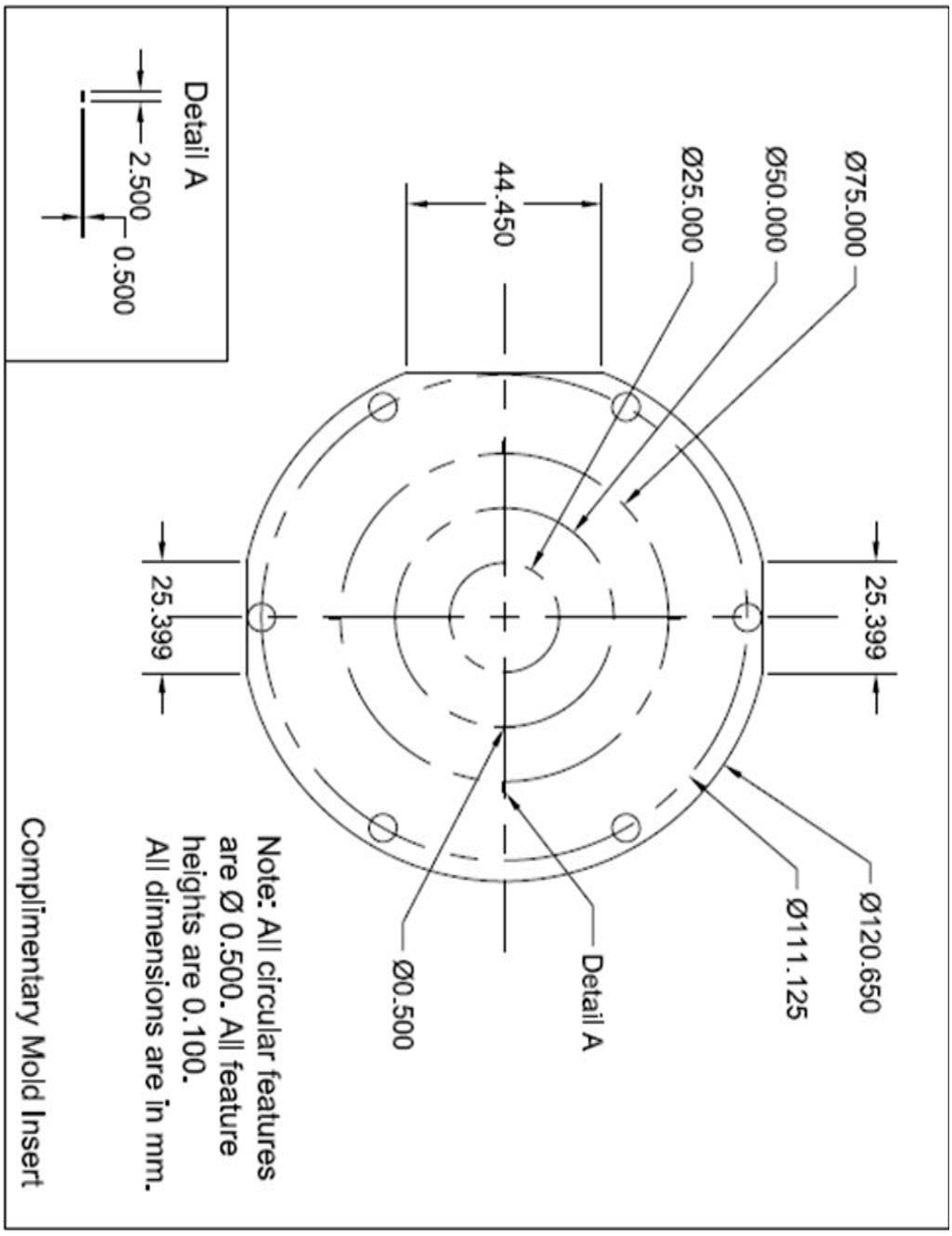

Drawing of Complimentary Mold Insert showing all critical dimensions of features.

REFERENCES

Blanding, D. L. (1999). *Exact Constraint: Machine Design Using Kinematic Principles.* New York: ASME Press.

Downey, K., Parkinson, A., & Chase, K. (2003). An introduction to smart assemblies for robust design. *Research in Engineering Design*, 236-246.

Glinsner, T., Kreindl, G., & Kast, M. (2010). Nonimprint Lithography. *Advanced Optical Components, June*(2), 42-45.

Glinsner, T., Veres, T., Kreindl, G., Roy, E., Morton, K., Wieser, T., . . . Lindner, P. (2010). Fully automated hot embossing processes utilizing high resolution working stamps. *Microelectronic Engineering, 87*, 1037-1040.

Grund, T., Heckele, M., & Kohl, M. (2008). *Batch Fabrication Methods for Polymer Based Active Microsystems using Hot Embossing and Transfer Bonding Technologies.* Cardiff, UK: Whittles Publishing Ltd.

Heckele, M. (2004). Hot embossing - a flexible and successful replication technology for polymer MEMS. *Proceedings of SPIE*, 108-117.

Heckele, M., & Schomburg, W. K. (2004). Review on micro molding of thermoplastic polymers. *Journal of Micromechanics and Microengineering*, R1-R14.

Jiang, L., Pandraud, G., French, P. J., Spearing, S. M., & Kraft, M. (2007). A novel method for nanoprecision alignment in wafer bonding applications. *Journal of Micromechanics and Microengineering*, S61-S67.

Juang, Y.-J., Lee, L. J., & Koelling, K. W. (2002). Hot Embossing in Microfabrication. Part I: Experimental. *Polymer Engineering and Science*, 539-550.

Kastantin, M. J., Li, S., Gadre, A. P., Wu, L.-Q., Bentley, W. E., Payne, G. F., . . . Ghodssi, R. (2003). Integrated Fabrication of Polymeric Devices for Biological Applications. *Journal of Sensors and Materials*, 295-311.

Khan-Malek, C., Wood, R., Dudley, B., & Stadler, S. (1998). Multi-Level Exposures and 3-D X-ray Patterning for High-Aspect Ratio Microstructures. *Microelectrical Engineering*, 493-496.

Kim, J. Y., Baek, J. Y., Lee, K. A., & Lee, S. H. (2005). Automatic aligning and bonding system of PDMS layer for the fabrication of 3D microfluidic channels. *Sensors and Actuators A*, 593-598.

Mathur, A., Roy, S. S., Tweedie, M., Mukhopadhyay, S., Mitra, S. K., & McLaughlin, J. A. (2009). Characterisation of PMMA microfluidic channels and devices fabricated by hot embossing and sealind by direct bonding. *Current Applied Physics, 9*, 1199-1202.

Matteucci, M., Christiansen, T. L., Tanzi, S., Ostergaard, P. F., Larsen, S. T., & Taboryski, R. (2013). Fabrication and Characterization of injection molded multi level nano and microfluidic systems. *Microelectronic Engineering*, 294-298.

Skafte-Pedersen, P., Sip, C. G., Folch, A., & Dufva, M. (2013). Modular microfluidic systems using revesibly attached PDMS fluid control modules. *Journal of Micromechanics and Microengineering*, 1-10.

Slocum, A. H., & Weber, A. C. (2003). Precision Passive Mechanical Alignment of Wafers. *Journal of Microelectricalmechanical Systems*, 826-834.

Stoyanov, I., Tewes, M., Koch, M., & Lohndorf, M. (2006). Microfluidic devices with integrated active valves based on thermoplastic elastomers. *Microelectronic Engineering*, 1681-1683.

Tennico, Y. H., Koesdjojo, M. T., Kondo, S., Mandrell, D. T., & Remcho, V. T. (2010). Surface modification-assisted bonding of polymer-based microfluidic devices. *Sensors and Actuators B: Chemical*, 799-804.

Whitney, D. E. (2004). *Mechanical Assemblies: their design, manufacture, and role in product development.* New York: Oxford University Press.

You, B. H., Chen, P.-C., Park, D. S., Park, S., Nikitopoulos, D. E., Soper, S. A., & Murphy, M. C. (2009). Passive micro-assembly of modular, hot embossed, polymer microfluidic devices using exact constraint design. *Journal of Micromechanics and Microengineering, 19*(12), 1-11.